J 15.4

INTERANNUAL VARIAILITY OF TROPICAL CYCLONE ACTIVITY OVER THE EASTERN NORTH PACIFIC

PENG WU AND PAO-SHIN CHU*

Department of Meteorology, School of Ocean and Earth Science and Technology, University of Hawaii at Manoa, Honolulu, Hawaii

Abstract

On average, 16 tropical cyclones (TC) form over the eastern North Pacific (ENP) each year. During 1966 to 2003, the annual frequency ranges from 8 to 27, with a standard deviation above 4. The mechanism behind the interannual variability of TC activity is of interest. In this research, both accumulated cyclone energy (ACE) and TC occurrence frequency of each hurricane season (July, August, and September) are employed to represent TC activity. Two extreme events are selected with 1992 being the active and 1977 the inactive, during which large scale environmental parameters are compared.

Except sea surface temperatures (SSTs) being consistently warm and favorable, other environmental parameters, which include the vertical wind shear (VWS), low-level relative vorticity, and mid-tropospheric moisture content, experience substantial variation, and display much more favorable patterns for cyclogenesis in 1992 than in 1977. The Atlantic subtropical ridge extends further westward over the Gulf of Mexico and Central America during the 1992 hurricane season, enhancing the easterlies over the ENP. Meanwhile, a well-established monsoon trough is observed between the enhanced easterlies and cross equatorial westerlies. Additionally, negative meridional potential vorticity (PV) gradient is observed over the Caribbean in 1992, providing a more unstable upstream state. In 1992, reduced precipitation over the Caribbean and Central America is associated with the extension of the subtropical ridge, while increased precipitation over the ENP is likely to be brought by stronger TC activity. Compared with 1977, convective disturbances with 4-10-day time scale propagating from the east bring stronger convection in 1992. In both years, time series of the anomalous zonal wind over the cyclogenesis region oscillate with intraseasonal time scale, while TC formations do not necessarily conform to the peak westerly phases.

1. Introduction

The dynamics of cyclogenesis are quite nonlinear and complicated. Although a well-accepted and closed theory is absent, theoretical and observational studies have isolated a number of physical conditions that are important for cyclogenesis. Researches have further shown that the frequency and spatial distribution of TC formation are closely related to the climatology of some environmental parameters defined based on physical requirements for cyclogenesis.

Gray (1977) summarized six parameters to understand the seasonal climatology of cyclogenesis. These parameters include the Coriolis force, low level relative vorticity, vertical wind shear between upper and lower troposphere, SSTs, moist instability in terms of the vertical gradient of θ_e, and relative humidity of the middle troposphere. The product of these six parameters was referred to as the Seasonal Genesis Parameter (SGP).

The diagnosed seasonal cyclogenesis over the western North Pacific (WNP) derived by Gray (1977) using the SGP was quite similar with observation. Other studies have also shown skill using Gray's SGP. Watterson et al. (1995) examined the climatology and interannaul variation of global cyclogenesis with SGP derived from GCM simulation. Clark and Chu (2002) studied interannual variation of TC activity over the central North Pacific (CNP) by comparing the dynamic potential in SGP with the initial formation points of cyclogenesis.

Based on previous researches about cyclogenesis related with the seasonal climatology of large scale environment, we expect to understand the interannual variability of cyclogenesis over the ENP through comparing the seasonal climatology of those related environmental conditions. Section 2 introduces the data and methods employed in this study. Section 3 examines the interannual variability of

* *Corresponding author address:* Dr. Pao-Shin Chu, Department of Meteorology, School of Ocean and Earth Science and Technology, University of Hawaii at Manoa, 2525 Correa Road, Honolulu, HI 96822; e-mail: chu@hawaii.edu.

TC activity over the ENP. After a brief review of the ENP climatology in section 4, large scale environmental parameters related to the variation in TC activity are then examined in section 5. Discussion on contributions from several other features toward TC activity is given in section 6. The paper concludes in section 6.

2. Data and methodology

For TCs, we use the best track dataset for the ENP from Tropical Prediction Center (TPC)/National Hurricane Center (NHC). The dataset records 6-hourly (0000, 0600, 1200, 1800 UTC) center locations and intensities (maximum 1-minute surface wind speeds in knots) for all tropical storms (maximum sustained surface wind speeds between 34kt and 64kt) and hurricanes (winds at least 64kt) from 1966 through 2003.

Daily averaged wind data at 850, monthly mean winds, air temperature, specific humidity, geopotential height at multiple levels, 500mb relative humidity, and sea level pressure (SLP) are derived from the National Center for Environmental Prediction-National Center for Atmospheric Research (NCEP-NCAR) reanalysis dataset. The horizontal resolution of the reanalysis data is 2.5^{o} latitude-longitude.

Monthly mean SSTs are taken from National Oceanic and Atmospheric Administration (NOAA) Extended Reconstructed data provided by Climatic Diagnostic Center (CDC) in Boulder, Colorado. SST data are available with horizontal resolution of 2^{o} latitude-longitude.

Daily averaged outgoing longwave radiation (OLR) with 2.5^{o} latitude-longitude resolution is derived from NOAA Interpolated OLR dataset which is also provided by CDC. The temporal coverage is from 1974 to present, with data missing in 1978.

2.5^{o} latitude-longitude gridded monthly mean precipitation data is taken from Climate Prediction Center (CPC) Merged Analysis of Precipitation (CMAP). The temporal coverage of the data is from 1979 to present.

We calculate the tropospheric vertical wind shear between 200mb and 850mb following the equation

$$VWS = \left[\left(u_{200mb} - u_{850mb} \right)^2 + \left(v_{200mb} - v_{850mb} \right)^2 \right]^{1/2}$$

, where u and v denote the zonal and meridional wind components respectively.

The vertical component of the relative vorticity is calculated from the reanalysis wind fields with finite differentiation in the Grid Analysis and Display System (GrADS).

3. Interannual variability of TC activity over the ENP

Observation of TC is considerably poorer in the presatellite era compared to the postsatellite era over the ENP. We only examine the period from 1966 to 2003 in this study as satellite operation started from the 1960s over this domain.

An annual average of around 16 TCs was reported during 1966 to 2003, while the annual cycle of cyclogenesis is pronounced. We could learn from Fig. 1 that TCs only occur from May through November, while those occurring in July, August, and September (JAS) accounts for more than 70% of the total. Thus, JAS is considered as the peak hurricane season in this research, and seasonal mean environmental parameters analyzed in the following sections will refer to the averaged values through these three months.

In order to quantify the interannual variability of TC activity, we calculate the ACE, an index that combines the frequency, duration, and intensity of each TC occurring over a basin during a given period of time. The ACE index is defined as the sum of squares of the estimated 6-hourly maximum sustained wind speed (knots) for all named systems while they are at least of tropical storm strength.

Time series of ACE during each hurricane season from 1966 to 2003 is shown in Fig. 2. Constructed based on the squares of maximum wind speeds, ACE weights more on TC intensity than on frequency and duration, which makes this study of interannual variability more meaningful as stronger cyclones have greater potential to cause severe damage.

According to the time series in Fig. 2, we choose 1977 with the minimum ACE and 1992 with the maximum ACE as two extremes to study the interannual variability. Moreover, on the time series of TC occurrence frequency during each hurricane season from 1966 to 2003 in Fig. 3, 1977 and 1992 also stand out beyond one standard deviation from the average. Thus, these two cases bear enough significance in representing the variability of TC frequency, intensity and duration.

4. Climatology of the large scale environment over the ENP

Before starting to investigate the large scale environmental variation related to the interannual variability of TC activity, it would be necessary to establish a background based on the climatology of the environment, which could be used later as the reference to evaluate the variation.

The majority of the ENP TCs form over a small region over warm SST to the west of Central America, approximately from 90^{o}W to 120^{o}W and from 10^{o}N to 20^{o}N. As shown in Fig. 4, the climatological seasonal mean SSTs beneath this region circled by dashed lines are well above 26^{o}C, which provides one of the favorable conditions for cyclogenesis. McBride (1995) has suggested that the highest frequency of TC genesis per unit area in the world is found over a compact region in the ENP with SST above 29^{o}C.

By observing other variables in Fig. 4, one could find that the area of warm SSTs coincides with that of low pressure and confluence between the northeasterly trades and the cross equatorial southwesterly flow, while all collocating within the cyclogenisis region. The confluence region, named after Intertropical Convergence Zone (ITCZ), extends from the cyclogenesis region toward the southwest following the warm SSTs of greater than 28^{o}C. At the same location as the ascending branch of the Hadley cell, warm SST provides constant buoyancy from the surface to support upward motion, which in turn lowers surface pressure. Meanwhile, confluence is forced by the local pressure gradient due to the lowered SLP.

Fig. 5 displays the seasonal climatology of OLR and CMAP precipitation over the ENP. With a close match of patterns between these two variables, large amount of precipitation occurs where strong convection is observed, over an area occupying the lower half of the cyclogenesis region. Additionally, this area of intense precipitation and strong convection is located identically as the ITCZ described in the last paragraph, which appears as a narrow zonal band of vigorous cumulus convection on satellite images.

In order to observe the three dimensional structure of the atmospheric circulation, latitude-height cross sections of 90^{o}W-110^{o}W averaged zonal and meridional winds are plotted against relative vorticity over the seasonal climatology in Fig. 6 and 7. At 1000mb, westerly and southerly winds corresponding to the cross equatorial flows dominate over areas to the south of 14^{o}N. To the north, easterlies and northerlies dominate over a wider latitudinal band until mid-latitudes. Southwesterlies gradually weaken with height and finally disappear near 850mb, while northeasterlies gradually strengthen and extend to the equator at levels above 850mb. Cyclonic relative vorticity is found along the boundary between the southwesterlies and northeasterlies, centered near 14^{o}N at 1000mb, and follows a southward tilted vertical axis, before turning into anticyclonic vorticity at 750mb. The anticyclonic vorticity dominates the entire mid and higher troposphere, and attains its maximum above 300mb over the cyclogenesis region between 10^{o}N and 20^{o}N.

Weak VWS between 200mb and 850mb is critical for TC formation and development. As shown in Fig. 6, persistent easterly winds in the troposphere, especially at levels higher than 850mb, produce weak VWS over the ENP. In Fig. 8, the climatological VWS weaker than 10 m s^{-1}, a crucial value for TC formation (Chu 2002), are observed over a large area including the cyclogenesis region.

At last, climatological relative humidity at 500mb, showing a quite similar pattern with that of OLR in Fig. 5, reaches its local maximums over the cyclogenesis region in Fig. 9. Specifically, large content of mid-tropospheric moisture supports climatological cyclogenesis over this certain area.

5. Variation of large scale environment

5.1 SST

TCs form and develop over regions of very warm sea surface where warm and moist air could support sustained deep convection and intense circulation. As shown in Fig. 4, SSTs are generally warm and favorable for cyclogenesis over the ENP. The standard deviation of seasonal mean SSTs from 1966 through 2003 is shown in Fig. 10a, with the dashed lines indicating the cyclogenesis region. Throughout the 38 years period, the lower boundary of the cyclogenesis region has a mean temperature above 26^{o}C which is considered as the threshold for TC formation. The standard deviation is about 0.4^{o}C, an extremely small variation making the climatological SSTs during JAS always favorable enough for cyclogenesis.

The difference of seasonal mean SSTs between 1992 and 1977 is negligible as shown in Fig. 10b, which suggests that the variability of SST is too weak to play an important role in causing significant change of TC activities between these two years. On the other hand, there must be other factors responsible for making the far more active 1992 hurricane season than the 1977 one.

5.2 Vertical wind shear

It is well known that weak vertical shear of the horizontal winds between upper and lower troposphere (typically between 850 and 200mb) is important for TC formation and development (Landsea 2000). Clark and Chu (2002) noted a substantial reduction of VWS to the south of Hawaiian Islands, which favors local TC activity in an El Nino composite. Likewise, Chu (2002) found reduced VWS related with increased TC activity in the study about decadal variation of TC activity over the central North Pacific (CNP).

The difference of seasonal mean VWS with 1992 minus 1977 is shown in Fig. 11. The negative values over the genesis region suggest that weaker VWS is present in the hurricane season of 1992, which is more favorable for cyclogenesis compared with the 1977 case. Additionally, the difference averaged over the genesis region is about 2 m s^{-1}, which accounts for approximately one third of the climatological seasonal average of about 6 m s^{-1} (Fig. 8). Thus, the variation of vertical wind shear is presumably large enough to explain the variability of cyclone activities between these two years.

Subsequently, we decompose the total VWS into components produced by only the zonal and meridional winds respectively, to see which one is more important causing the variation of VWS. Fig. 12a and b show the differences of the two components between 1992 and 1977. Comparing the absolute values over the genesis region in these figures, we could learn that the variation of the zonal shear is greater than that of the meridional shear from 1977 to 1992. Specifically, variation of the zonal shear makes the major contribution to change the total VWS.

Fig. 12c and d again plot the seasonal mean zonal shear during 1992 and 1977 to enhance our understanding. On both figures, negative values suggest the cyclogenesis regions experiences easterly shear, with winds at 200mb being more easterly than the 850mb winds. However, easterly shear is weaker during 1992 than 1977, which makes the difference positive in Fig. 12a.

Maloney and Hartmann (2000) have shown that, during westerly phase of MJO, more TCs occurred near areas of zero vertical shear of the zonal wind, with strong westerly shear to the north and strong easterly shear to the south. This pattern basically agrees with those found during the hurricane season in 1992 and 1977 on Fig. 12c and d, while areas of zero vertical shear locate closer to the genesis region during 1992 in Fig. 12c compared with the 1977 case in Fig. 12d.

In summary, vertical shear reduction of the zonal wind is the major contributor to reduce the total VWS from 1977 to 1992, while both features together favor cyclogenesis during 1992.

5.3 Low-level relative vorticity

As another critical environmental factor for cyclogenesis, low-level relative vorticity at 925mb is shown in Fig. 13 for the hurricane seasons in 1992, 1977, and their difference as the prior minus the latter. Fig. 13a shows an elongated belt of strong cyclonic vorticity with values greater than 5×10^{-6} S^{-1} overlaying the majority of the cyclogenesis region, in which solid dots indicating the initial detection locations. The enhanced low-level cyclonic vorticity in 1992 which presumably favors TC formation, is consistent with the well defined monsoon trough which will be discussed in the later part.

In the 1977 hurricane season, low-level cyclonic vorticity is not as well organized as that in 1992, and appears vague around the longitude of 100^{o}W as shown in Fig. 13b. A westward shift of the cyclogenesis locations by 5^{o} longitudes from 1992 toward 1977 is noticed when comparing the centroid genesis location denoted by the crosses in Fig. 13a and b. This westward shift is quite likely due to the fact that cyclonic vorticity in 1977 is only present over the western end of the climatological genesis region.

Difference in Fig. 13c again reveals the significant variation in the low-level relative vorticity, with values up to 8 $\times 10^{-6}$ S^{-1} over the genesis region which double the seasonal climatology in Fig. 6 and 7. Specifically, it is the enhanced (reduced) cyclonic vorticity over the genesis region in the 1992 (1997) hurricane season that favors (inhibits) TC formation.

To address the question that whether cyclonic vorticity is a contribution to cyclogenesis or is produced by TC activity itself, we first hypothesize that cyclones produce areas of cyclonic vorticity following their development and movement. Under this hypothesis, we would expect to locate areas of cyclonic vorticity preferentially downstream of the genesis region, since TCs usually reach their maximum intensity several days after formation. However, it is not the case in Fig. 13a and b, in which areas of strong cyclonic vorticity are found within cyclogenesis region, instead of over downstream region. Thus, the hypothesis should be rejected, and cyclonic vorticity should be considered as the cause rather than the effect of TC activities.

5.4 Mid-tropospheric moisture content

Mid-tropospheric moisture content is directly related to tropical cyclogenesis. Drier mid-troposphere tends to suppress deep cumulus convection, while large content of moisture at the mid-troposphere could enhance deep cumulus convection by reducing entrainment drying of the updraft, which makes cumulus convection more likely to develop into TC strength.

Fig. 14 shows that the difference of seasonal mean 500mb relative humidity over the cyclogenesis region is around 13% when the 1977 value is subtracted from the 1992 one, accounting for about one fourth of the long term seasonal average which is around 50% in Fig. 9. Thus, significant larger content of mid-tropospheric moisture in 1992 favors cyclogenesis compared with the 1977 case.

One of the parameters related with climatological cyclogenesis given by Gray (1977) is the moist instability in terms of the vertical gradient of θ_e. To measure the instability, we employ the moist static energy which has analogous physical meaning as θ_e, that is the temperature of one parcel of air at 1000mb after considering the energy from when the water vapor in the parcel is condensed. The moist static energy is calculated by $C_pT+gz+L_vr$, which is the sum of the enthalpy, gravitational potential energy, and latent heat content of an air parcel. The vertical profile of the seasonal mean moist static energy averaged over 90°W to 110°W and 10°N to 20°N is plotted in Fig. 15.

During both hurricane seasons of 1992 and 1977, the troposphere below 700mb shows equally conditional instability with $\partial\theta_e / \partial p$ being positive. However, moist static energy in 1992 becomes greater than that in 1977 starting from 700mb, and their difference attains its maximum at 500mb, which is consistent with the significantly different relative humidity at this level shown in Fig. 14. Given the comparable moist instability between these two years, it is the different mid-tropospheric moisture content that plays the critical role related to the variability of TC activity.

5.5 PV on 310K isentropic surface

It is frequently stated that cyclogenesis in the ENP occurs in association with easterly waves that have propagated from Africa across the Atlantic and Caribbean (Avila 1991). Burpee (1972) showed that these waves had developed over Africa where the negative meridional gradient of PV near 700mb offered an unstable basic state. Similarly, an area of negative meridional PV gradient at the lower troposphere over the Caribbean in the 1991 summer, indicated with a box in Fig. 16, was discovered by Molinari (1997). In that article, it was shown that the magnitude of the PV gradient, along with the ENP cyclogenesis, varied on the timescale of Madden-Julian oscillation (MJO) during the 1991 summer. It was also suggested that the negative PV gradient offered an unstable basic state to reinvigorate easterly waves propagating westward which later lead to subsequent cyclogenesis, and that the modulation of the PV gradient by MJO caused the intraseasonal variability of downstream cyclogenesis in 1991.

Here we compare the seasonal averaged PV between 1992 and 1977. Following Molinari (1997), PV is calculated on 310K isentropic surface lying between 725mb and 825mb over the areas of interest, given by the form $q = g\left(-\frac{\partial p}{\partial \theta}\right)^{-1}\left(\zeta_\theta + f\right)$ in which air pressure p and vertical component of relative vorticity ζ are linearly interpolated to isentropic surfaces.

Fig. 17 displays the seasonal mean 310K PV in 1992 and 1977, in which areas with values greater than $2.5\times10^{-7}m^2Ks^{-1}kg^{-1}$ are shaded. An area of negative PV gradient is found near 85°W and 20°N in Fig. 17a, suggesting an unstable basic state in the 1992 hurricane season which presumably favors easterly waves invigoration and subsequent cyclogenesis. Such condition is not available in the 1977 hurricane season from Fig. 17b, which is consistent with the less active hurricane season in this year.

Based on these observations, the interannual variation of PV seasonal climatology would then play an important role in causing the variability of TC activities in the ENP. However, the process that easterly wave disturbance developing into TC strength passing the negative PV gradient region needs to be verified, such that the connection between the cause and effect could become better understood.

5.6 Monsoon trough over ENP

Previous studies have shown that spatial distribution and frequency of cyclogenesis are generally governed by the location and intensity of the monsoon trough on a seasonal mean time scale. Being a convergence zone between trade easterlies and cross equatorial southwesterlies, monsoon trough could produce low-level cyclonic vorticity and weak vertical wind shear which support favorable environmental condition for cyclogenesis.

Fig. 18 plots the streamline analysis based on seasonal mean winds at 925mb during the hurricane seasons of 1992 and 1977. In Fig. 18a, a well-established monsoon trough marked by the bold solid curve is observed in 1992 extending zonally over the cyclogenesis region, while monsoon trough is absent or at least not well defined from the seasonal climatology of 1977 in Fig. 18b.

Given the presence of a well defined monsoon trough in 1992, it is consistent that we have observed stronger cyclonic vorticity (Fig. 13) and weaker VWS (Fig. 11 and 12) within the same area. These favorable environmental conditions together support stronger TC activities in 1992 compared with 1977.

By comparing the streamline analysis in 1992 and 1977, two major differences in the circulation neighboring the monsoon trough are observed. First, the easterlies crossing the Central America show a pronounced ridge around 100°W on the poleward side of the monsoon trough only in 1992. Although 925mb streamline analysis should be masked out over some parts of the continent due to the elevated topography, the ridge in the easterlies still dominate over the ocean off the western coast of Central America. We speculate that the mechanism of land-air interaction over Central America and the extension of Atlantic subtropical ridge might contribute to the formation of this circulation pattern associated with the monsoon trough in 1992. This speculation will be evaluated by studying the subtropical ridge and precipitation in the following parts.

Second, there are much stronger monsoon westerlies in the cross equatorial flow between the latitudes of 5^{o}N and 10^{o}N in 1992 than in 1977. Specifically, the cross equatorial southerly flow recurves into westerlies by the Coriolis force more rapidly in 1992. The stronger monsoon westerlies in 1992 are revealed more clearly by comparing the zonal winds as follows.

Fig. 19 shows a striking difference when the seasonal mean zonal winds at 925mb of 1977 are subtracted from those of 1992. When the monsoon trough is present, stronger easterlies are found extending westward from the Caribbean into the ENP along the latitudes between 10^{o}N and 20^{o}N, while stronger westerlies exist to the south of the stronger easterlies. The position of the monsoon trough observed in 1992 is denoted here with a bold curve. From this scenario, stronger easterlies to the north and stronger westerlies to the south are considered as key components of a better-established monsoon trough.

It is further noticed that the difference of zonal wind reaches below -2.5m s^{-1} in the easterlies over a certain area of the ENP, which exceeds the climatological wind speeds shown in Fig. 6 at this level. The difference in the monsoon westerlies is less significant, but still equals the climatology.

6. Discussion

A number of parameters studied above have consisted of a favorable (unfavorable) large scale environment for cyclogenesis in the 1992 (1977) hurricane season. To some extent, these parameters are all directly related to the physical requirement for cyclogenesis. During the following parts, we will discuss several other features that might have caused the variations of those parameters between the two extreme years.

6.1 Westward extension of subtropical ridge over the Atlantic

Following earlier speculation about the formation of monsoon trough, we now investigate the influence from the Atlantic subtropical ridge on the circulation over the ENP and Central America, by analyzing the seasonal mean geopotential height and wind at 925mb of 1992, 1977, and their difference.

Comparing Fig. 21a and b, a westward extension of subtropical ridge is detected during 1992 between the longitudes of 55^{o}W and 70^{o}W over the Atlantic. In Fig. 21c which shows the difference, this westward extension of high pressure brings more easterlies and stronger anticyclonic flow over the western Atlantic during 1992. However, anticyclonic flow over this region is too distant to directly contribute to the circulation over Central America and the ENP.

Another area affected by the westward extension of subtropical ridge in 1992 is over the Gulf of Mexico. This is depicted more clearly in Fig. 21c where an area of positive difference of geopotential height and anticyclonic difference of the circulation is centered near 20^{o}N and 90^{o}W. The extension of subtropical ridge over this area is believed to be responsible for the aforementioned circulation features during 1992 including the easterly ridge in Fig. 18a and stronger easterlies in Fig. 19 over Central America and ENP.

In summary, the westward extension of subtropical ridge over the Gulf of Mexico in the 1992 hurricane season contributes, in part, to a favorable circulation pattern of a well-established monsoon trough downstream over the ENP.

6.2 Precipitation

We have shown that air pressure and circulation fields experience significant variation from active to inactive years of TC activity. As another evidence to support this point, it is of interest to investigate the variation of precipitation, which could also reflect the effects of circulation change more completely.

Fig. 22 displays the seasonal mean CMAP precipitation in 1992, 1979 and their difference. Because CMAP precipitation data is only available from 1979, here we employ 1979 as the inactive case of cyclone activity to make up the data unavailability for 1977. From Fig. 3, frequency of TC occurrence in the 1979 hurricane season equals that in 1977. Moreover, the ACE in 1979 is the second lowest after 1977, during the 38 years period in Fig. 2. Thus, the hurricane season of 1979 should be representative enough as an inactive case as that of 1977.

Similar as Fig. 5, the precipitation during the hurricane seasons in Fig. 22a and b mainly concentrates over an area along 10^{o}N between 80^{o}W and 120^{o}W. Located on the southern edge of the cyclongenesis region, this area of intensive precipitation is related with the ITCZ.

By observing the difference of precipitation in Fig. 22c, we find the Caribbean and Gulf of Mexico is significantly drier during 1992 than 1979. Over this domain, precipitation in 1979 doubled the value in 1992 when comparing Fig. 22b with a.

In Fig. 22c, another area of significantly less precipitation in 1992 hurricane season is over Central America around 17^{o}N and 97^{o}W. This is associated with the easterly ridge in Fig. 18a and higher pressure in Fig. 21c over the corresponding area.

Although the variation of precipitation does not directly cause the variability of TC activity over the ENP, both of them are shown to be associated with the variation of circulation. We investigate variation of precipitation here to get a more complete picture of what could be resulted from the variation of circulation.

Over the Pacific region, more precipitation in 1992 is found to the west of 110^{o}W between 10^{o}N and 20^{o}N. Since this area is dominated by the northeasterly trade wind and experiences much less precipitation compared with the ITCZ region, larger precipitation in 1992 is quite likely to be brought by stronger TC activity in that year.

6.3 Westerly winds associated with the monsoon trough

Following previous discussion about stronger easterlies on the poleward side of the monsoon trough (Fig. 19) produced by the westward extension of the Atlantic subtropical ridge, we next examine the mechanism responsible for stronger westerlies on the equatorward side of the monsoon trough.

Research by Maloney and Hartmann (2000) has suggested that the westerly wind bursts over the ENP which are favorable for cyclogenesis is caused by the Madden-Julian Oscillation (MJO). On intraseasonal timescale, MJO modulates cyclogenesis while alternating low-level easterly and westerly winds over the areas between the equator and 15^{o}N. The composited zonal wind anomalies based on westerly phase shows similar pattern as the difference of seasonal mean zonal winds between 1992 and 1977 in Fig 19, with westerly anomalies to the south of easterly anomalies. Here we want to examine whether the stronger westerly wind blowing to the south of the monsoon trough in the 1992 hurricane season is caused by MJO.

Because MJO has strongest low-level signal at 850mb (Madden and Julian 1994), we show in Fig. 20 that zonal wind differences at this level is not only comparable with, but even greater than that at 925mb shown in Fig. 19. Although monsoon trough and cross equatorial flows are absent at 850mb, the barotropic structure in Fig. 20 suggest that circulation at this level is consistent with lower level circulation producing a well-defined monsoon trough in 1992.

In order to follow the characteristic periods of MJO, a 30-50-day bandpass filter is first used toward zonal winds at 850mb. Variances of the filtered zonal winds during the hurricane seasons are plotted in Fig. 23, where locations of large variances conform well to that of westerly difference of the zonal wind in Fig. 19. However, during 1992 the maximum variance is located more northwestward compared with that during 1977. Meanwhile, areas of large variances extend more eastward in 1992 than in 1977 when comparing the 6 $m^2 s^{-2}$ contour, suggesting that larger amplitude of zonal wind variation over a wider domain is related with stronger TC activity.

In Fig. 24, time series of the 30-to-50-day filtered zonal wind anomalies during June to October over locations of the maximum variances denoted by the solid dots in Fig. 23 show oscillation with period of MJO time scale. In both 1992 and 1977, westerly wind anomalies occur around mid-August and late September, while easterly anomalies occur during early September and mid-October. Although zonal wind anomalies show similar progressing pattern between two years, cyclogenesis indicated by solid squares occurs much more frequently in 1992 than in 1977. Additionally, cyclogenesis in 1992 tends to be widespread instead of being clustered and preceded by the peak of westerly anomalies. Similarly in 1977, cyclogenesis starts during mid-September while zonal wind is still in easterly anomalies.

If the case here is that westerly wind bursts lead to cyclogenesis, then we would expect a totally different scenario where cyclogenesis would cluster and be preceded by the peak of westerly anomalies. However, this is apparently not the case in Fig. 24, thus westerly wind bursts should not be taken as the direct cause of cyclogenesis.

To support this point, we plot in Fig. 25 the time-longitude cross section of the 30-50-day filtered 850mb zonal wind anomalies along the latitudes of the maximum variances in 1992 and 1977. In both panels, shadings indicating the westerly anomalies do not precede in time the TC formation, especially for the strong westerly anomalous events around July 16, August 20, and September 16 in 1992. Besides, westerly anomalies with comparable, or even large, amplitudes and extension in time and physical dimension occurred in the 1977 hurricane season, while cyclogenesis is significantly weaker.

From observation and analysis above, we attribute the peaks of westerly wind to cyclone activities, rather than taking those as mechanism to support cyclogenesis. Given the MJO-like period of the 850mb zonal wind anomalies, it still lacks evidence to say they are directly related with MJO.

6.4 Convection

In this section we compare the convection in terms of the OLR in the hurricane seasons of 1992 and 1977, on both seasonal mean state and transient state.

Fig. 26 shows the difference of seasonal mean OLR when the 1977 value is subtracted from the 1992 one. Lower values of OLR, which suggest stronger convection activity, are observed during 1992 over a large domain including the cyclogenesis region. Areas with the most significant difference, instead of being located along the track of TCs, are found over the eastern end of the cyclogenesis region, along 90^{o}W off the western coast of Central America. This suggests that stronger convection during 1992 should be considered as a favorable background for TC formation, rather than as a product of a more active hurricane season.

Next to the cyclogenesis region, stronger convection is also observed over Central American continent between the latitudes of 10^{o} and 20^{o} N during 1992, with considerable extension to the Caribbean and Gulf of Mexico.

Corresponding to stronger convection in 1992 compared with 1977 on the seasonal mean state, larger amplitudes of convective disturbance is also observed in 1992 from Fig. 27, which shows the difference when variances of OLR during the 1977 hurricane season are subtracted from those during 1992. It is of primary interest here to find out which processes have caused stronger convective activity in 1992, given a favorable environment for cyclogenesis as shown in section 4.

Spectral analysis allows us to determine which frequency component in time series plays the leading role by supporting the largest part of energy to the overall disturbance. Following the method of Chu and Katz (1989), spectral density functions versus periods are calculated based on time series of OLR during June-October over a number of locations, which experience both stronger seasonal mean convection and larger variance during 1992. In Fig. 28, time series of OLR over 12.5^{o}N, 90^{o}W and 12.5^{o}N, 85^{o}W are dominated by disturbance with periods of 4-7-day, while time series over 12.5^{o}N, 100^{o}W and 22.5^{o}N, 95^{o}W are dominated by 5-10-day disturbance. Thus, it becomes evident that synoptic scale disturbance with 4-10-day periods is the major component in causing the large variation in convective activity from 1977 to 1992.

Subsequently, longitude-time series of 4-10-day filtered OLR anomalies averaged between 10-20^{o}N are plotted for June to October during 1992 and 1977 in Fig. 29. In both panel a and b, each convective disturbance passing over the cyclogensis region could be traced back to 80^{o}W or further eastward. Meanwhile, each TC formation is preceded by such westward propagating convection package.

Based on these features, we suggest that it is the 4-10-day convective disturbance propagating from the east of the cyclogenesis region that has caused much more active convection in the 1992 hurricane season. And such convective activity in 1992, together with a favorable large scale environment, has lead to a hurricane season with more frequent and stronger TC activity.

7. Conclusion

Large scale environmental conditions during the hurricane seasons are compared between 1992 and 1977, which experience respectively the most active and inactive TC activity during a 38 years period. While SSTs are consistently warm and favorable, other environmental parameters such as the VWS, low-level relative vorticity, and mid-tropospheric moisture content experience substantial variation between the two extreme years, displaying much more favorable patterns for cyclogenesis in 1992 than in 1977. Upstream of the cyclogenesis region, an unstable state with negative meridional PV gradient is present over the Caribbean only in 1992. Additionally, the Atlantic subtropical ridge extends westward over the Gulf of Mexico and Central America in the 1992 hurricane season, enhancing the easterlies over the ENP. Meanwhile, a well-established monsoon trough over the TC genesis location is observed between the enhanced easterlies and cross equatorial westerlies. In 1992, reduced precipitation over the Caribbean and Central America is associated with the extension of subtropical ridge, while increased precipitation over the Eastern North Pacific is likely to be brought by stronger TC activity. Compared with 1977, synoptic scale convective disturbances with 4-10-day periods propagating from the east bring stronger convection on both seasonal mean and transient states in 1992. In both years, time series of the anomalous zonal wind over the cyclogenesis region oscillate with intraseasonal time scale, while TC formations do not conform to the peak westerly phase.

References

Avila, L. A., 1991: Eastern North Pacific hurricane season of 1990. *Mon. Wea. Rev.*, 119, 2034-2046.

Burpue, R. W., 1972: The origin and structure of easterly waves in the lower troposphere of North Africa. *J. Atmos. Sci.*, 29, 77-90.

Chu, P.-S., 2002: Large-scale circulation features associated with decadal variations of tropical cyclone activity over the Central North Pacific. *J. Climate*, 15, 2678-2689.

Chu, P.-S. and R. W. Katz, 1989: Spectral estimation from time series models with relevance to the Southern Oscillation. *J. Climate*, 2, 86-90

Clark, J. D., and P.-S. Chu, 2002: Interannual variation of tropical cyclone activity over the central North Pacific. *J. Meteor. Soc. Japan*, 80, 403-418.

Gray, W.M., 1977: Tropical cyclone genesis in the western North Pacific. *J. Meteor. Soc. Japan*, 55, 465-482.

Landsea, C. W., 2000: El Nino-Southern Oscillation and seasonal predictability of tropical cyclones. *El Nino and the Southern Oscillation: Multiscale Variability and Global and Regional Impact*s, H. F. Diaz and V. Markgraf, Eds., Cambridge University Press, 149-181.

Madden R. A., and P. R. Julian, 1971: Observations of the 40-50-day tropical oscillation – a review. *Mon. Wea. Rev.*, 12, 814-837.

Maloney, E. D., and D. L. Hartmann, 2000: Modulation of eastern North Pacific hurricanes by the Madden-Julian oscillation. *J. Climate*, 13, 1451-1460.

McBride, J. L., 1995: Tropical cyclone formation. *Global Perspectives on Tropical Cyclones*, R. L. Elsberry, Ed., WMO Tech. Document 693, 63-105.

Molinari, J., D. Knight, M. Dickison, D. Vollaro, and S. Skubis, 1997: Potential vorticity, easterly waves, and tropical cyclogenesis. *Mon. Wea. Rev.*, 125, 2699-2708.

Watterson, I. G.., J. L. Evans, and B. F. Ryan, 1995: Seasonal and interannual variability of tropical cyclogenesis: diagnostics from large-scale fields. *J. Climate*, 8, 3052-3

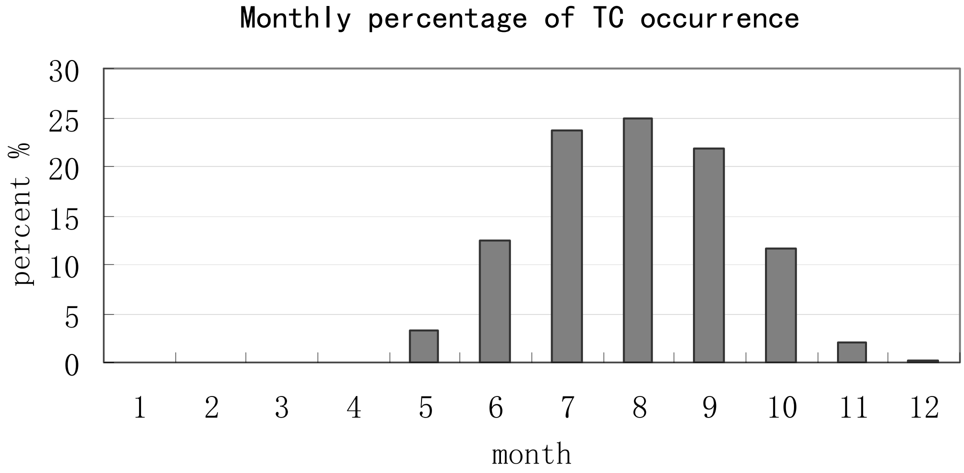

Fig. 1. Monthly percentage of TC occurrence relative to annual total during 1966-2003

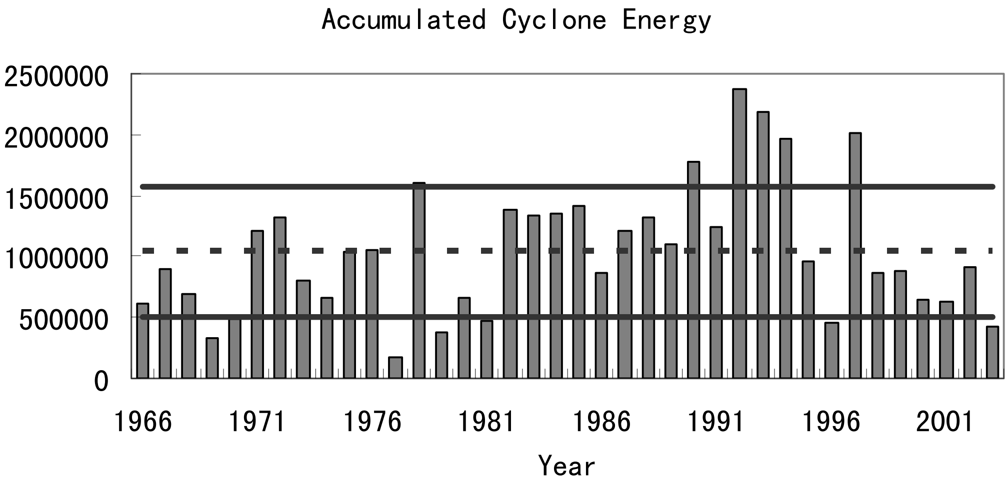

Fig. 2. Seasonal (JAS) ACE (square knots) during 1966-2003. Dashed line denotes the mean. Solid lines denote the mean plus and minus one standard deviation respectively.

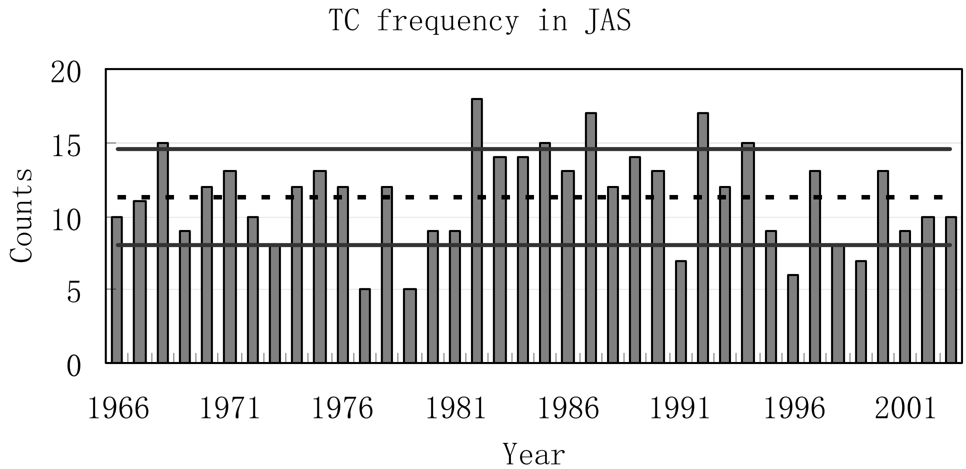

Fig. 3. Same as Fig. 3, except for TC occurrence frequency during 1966-2003.

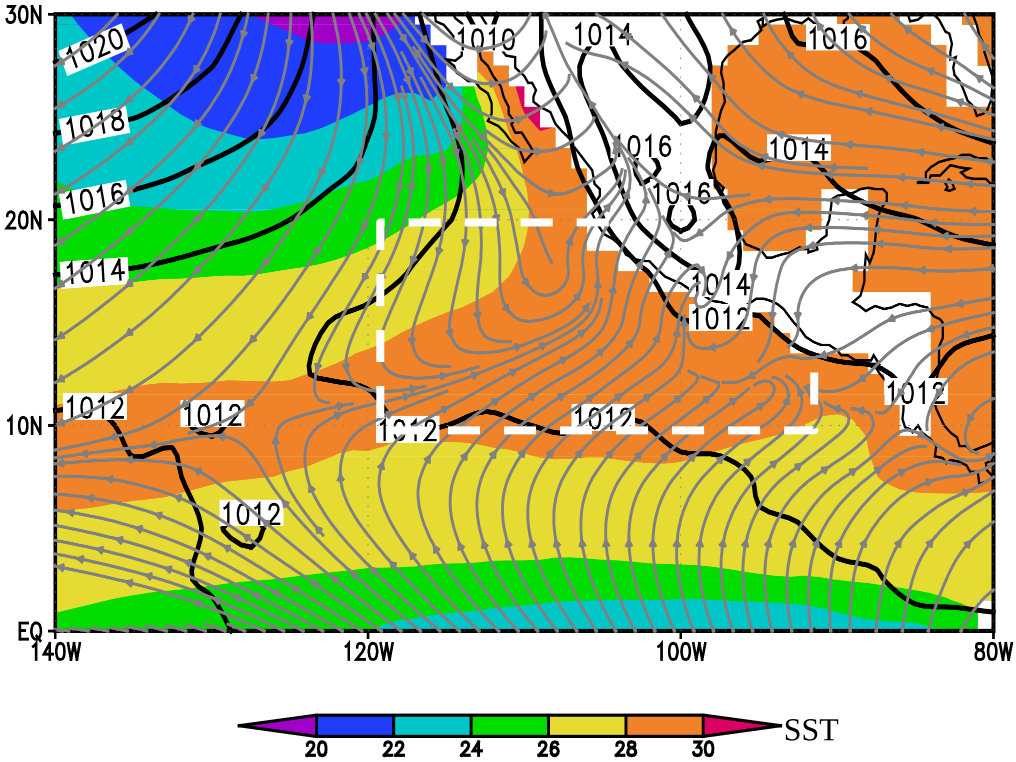

Fig. 4. Climatological (1966-2003) seasonal mean fields, where shadings denote SST (^oC) values and contours denote SLP (mb) values, overlaid with surface streamline analysis. Dashed lines circle cyclogenesis region.

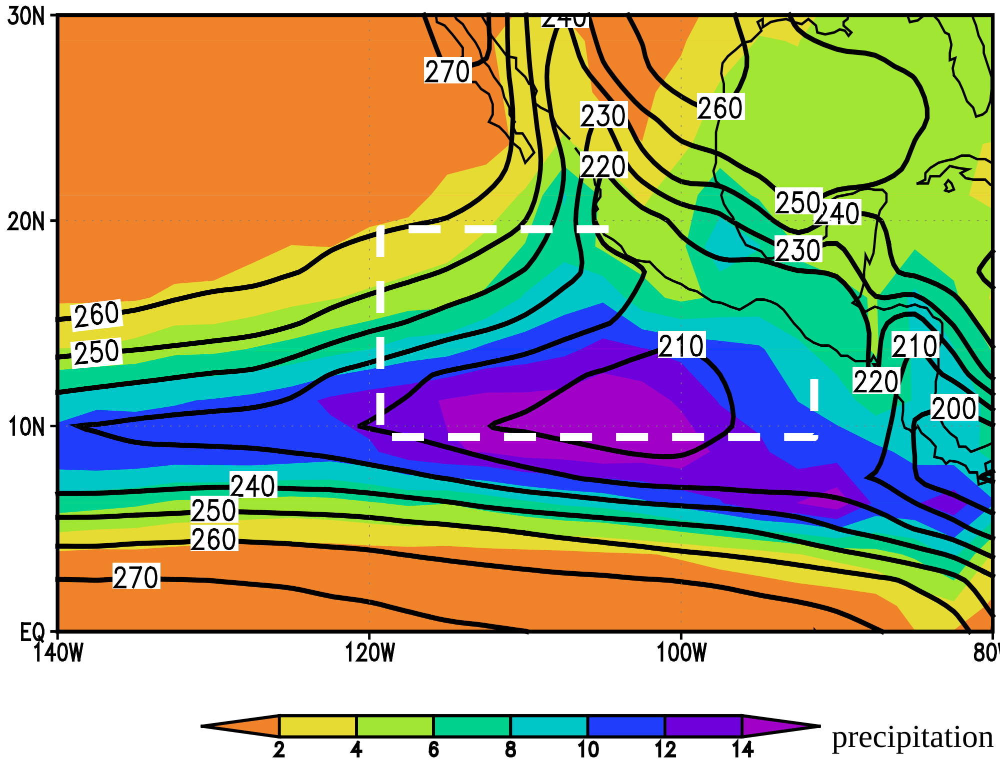

Fig. 5. Same as Fig. 4, except shadings denote values of precipitation (mm day^{-1}), and contours denote values of OLR (W m^2).

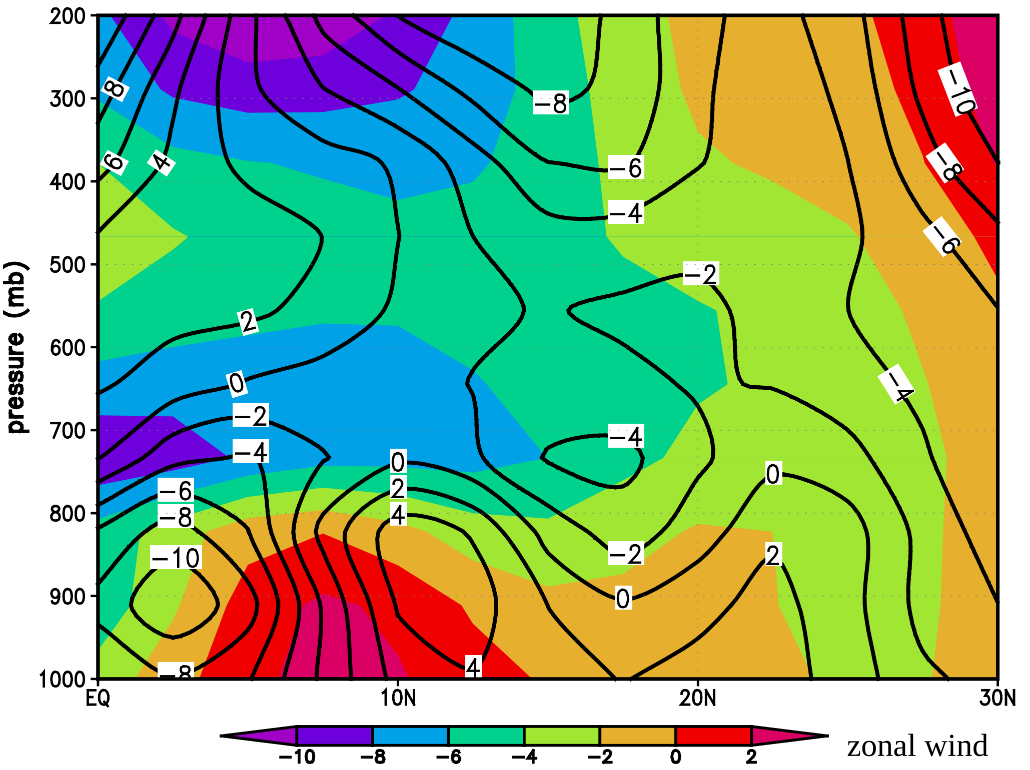

Fig. 6.Latitude-height cross section of climatological (1966-2003) seasonal mean fields averaged between 90°W and 110°W. Shadings denote values of zonal wind (m s^{-1}), and contours denote values of relative vorticity (10^{-6} s^{-1}).

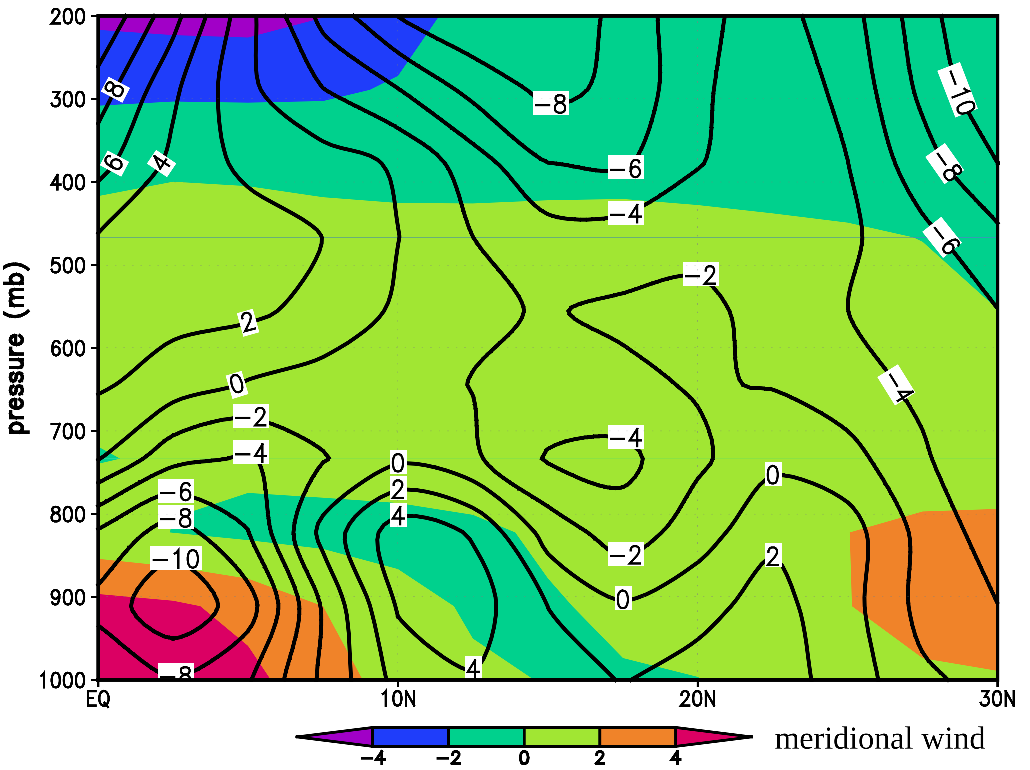

Fig. 7. Same as Fig. 5, except shadings denote values of meridional wind (m s^{-1}).

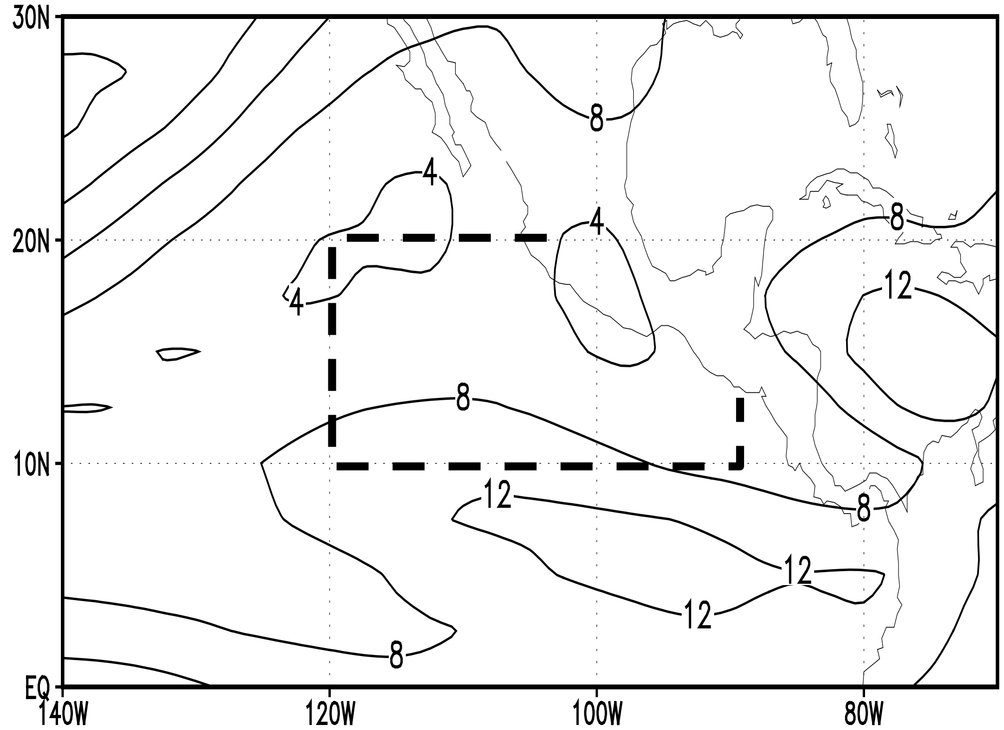

Fig. 8. Climatological (1966-2003) seasonal mean vertical wind shear (m s^{-1}) between 200mb and 850mb. Dashed lines circle cyclogenesis region.

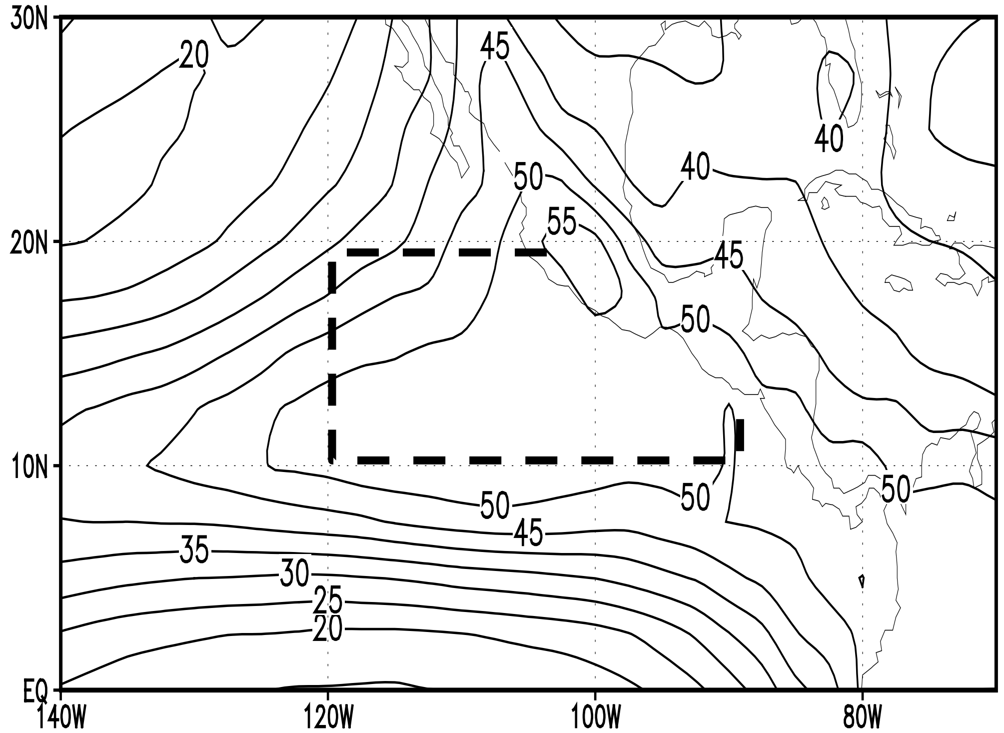

Fig. 9. Same as Fig. 8, except for relative humidity (%).

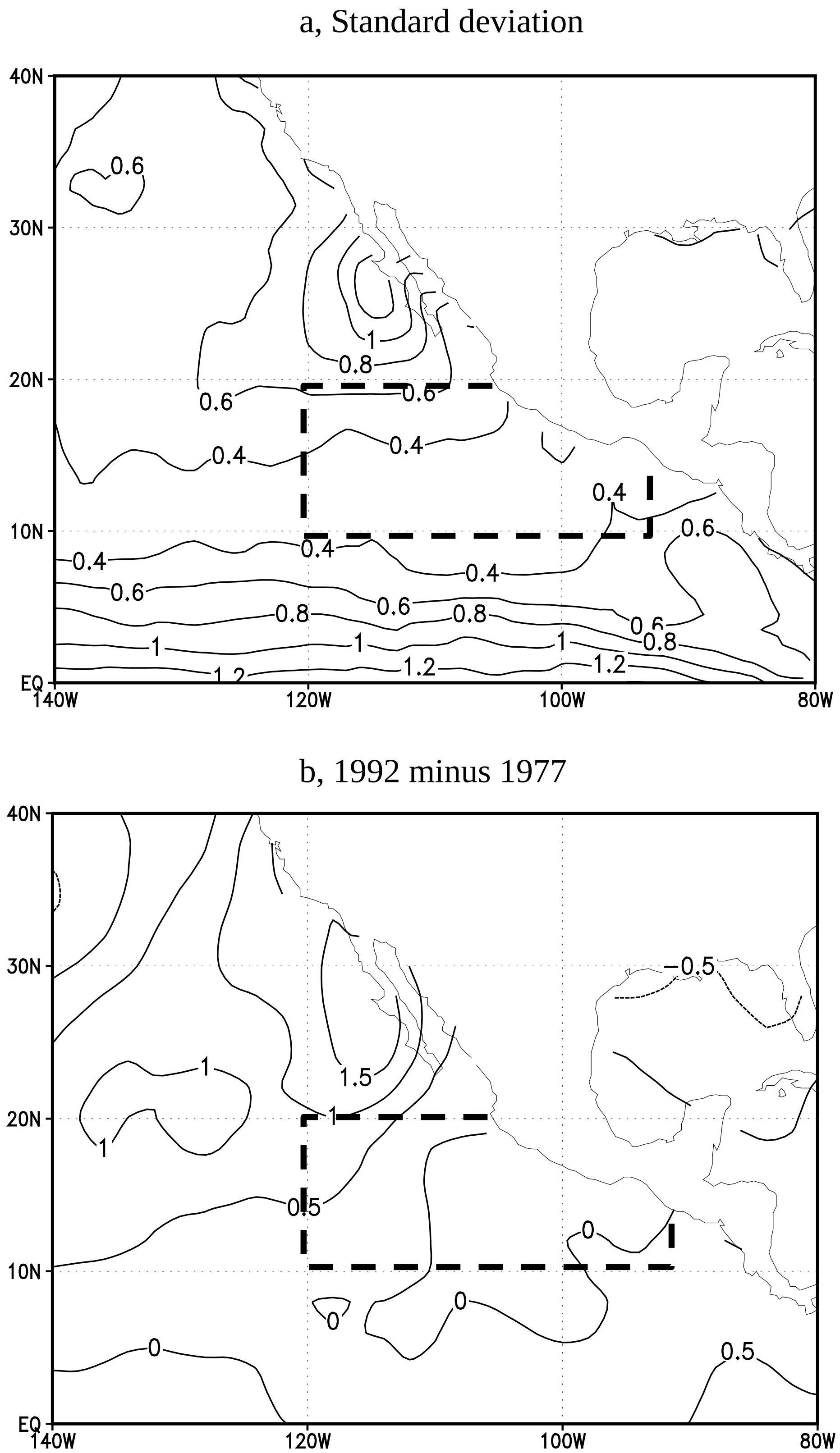

Fig. 10. (a) Standard deviation (1966-2003), and (b) 1992 minus 1977 seasonal mean SST (^{o} C). Dashed lines circle the cyclogenesis region.

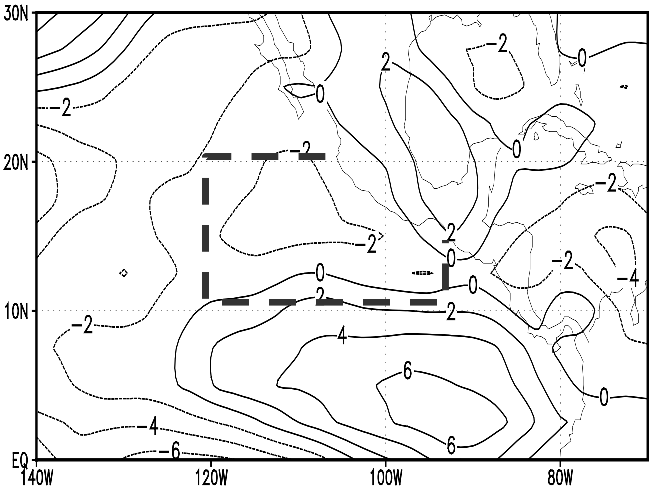

Fig. 11. 1992 minus 1977 seasonal mean vertical wind shear (m s^{-1}) between 200mb and 850mb. Solid (dashed) contours denote positive (negative) values. Dashed lines circle cyclogenesis region.

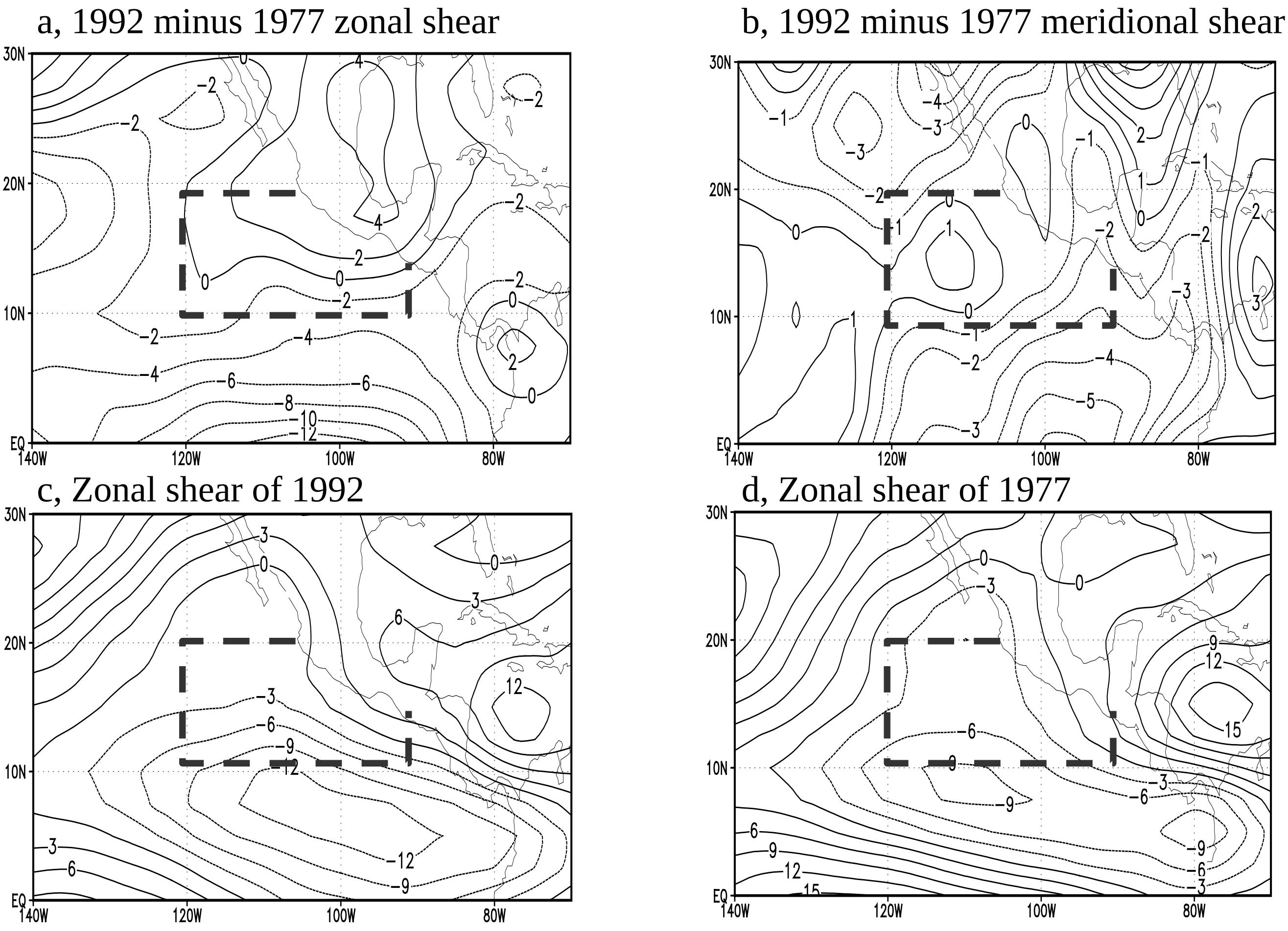

Fig. 12. Same as Fig. 11, except for 1992 minus 1977 (a) zonal, (b) meridional wind shear, and (c) 1992, (d) 1977 zonal wind shear.

a, 1992

b, 1977

c, 1992-1977

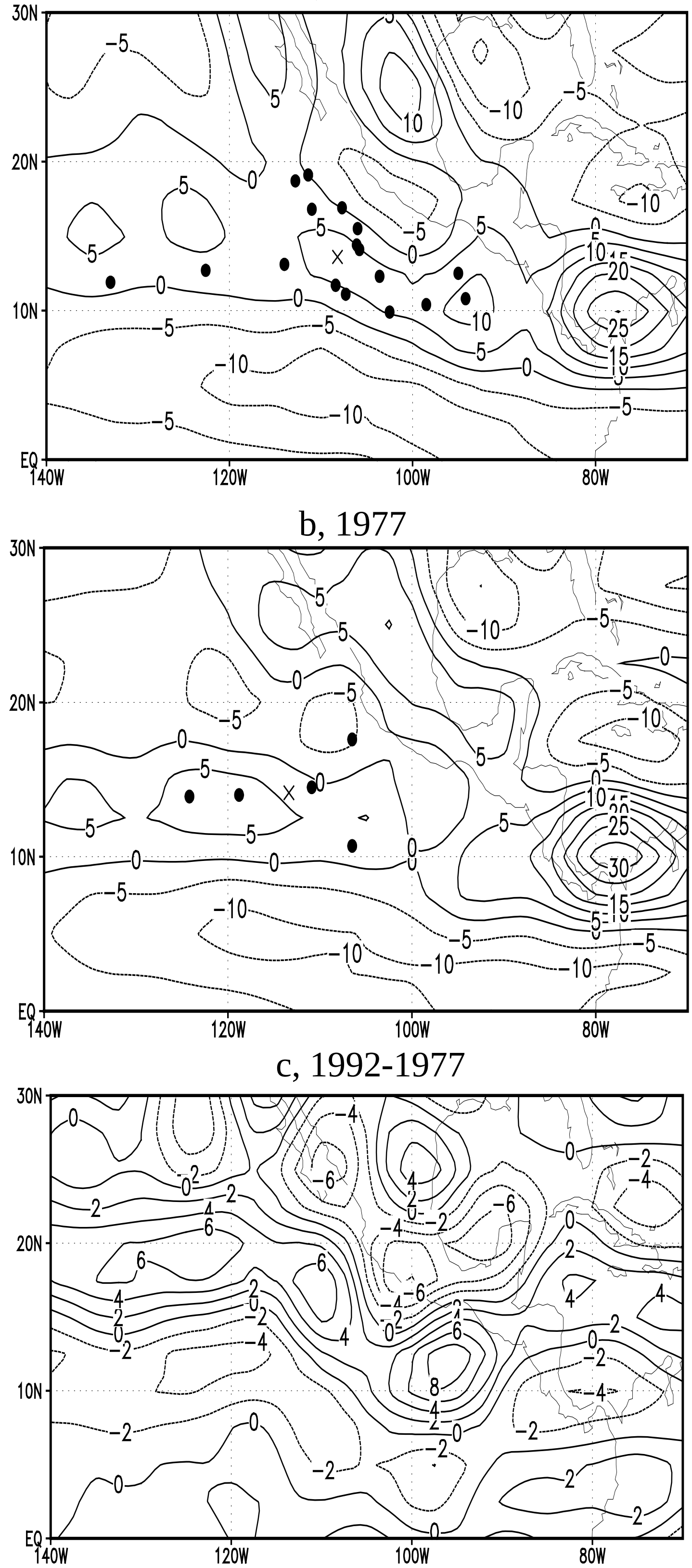

Fig. 13. Seasonal mean 925mb relative vorticity ($10^{-6}\,S^{-1}$) of (a) 1992, (b) 1977 and (c) 1992 minus 1977. Solid (dashed) contours denote positive (negative) values. Solid dots denote cyclogenesis locations, cross denotes the centroid genesis location.

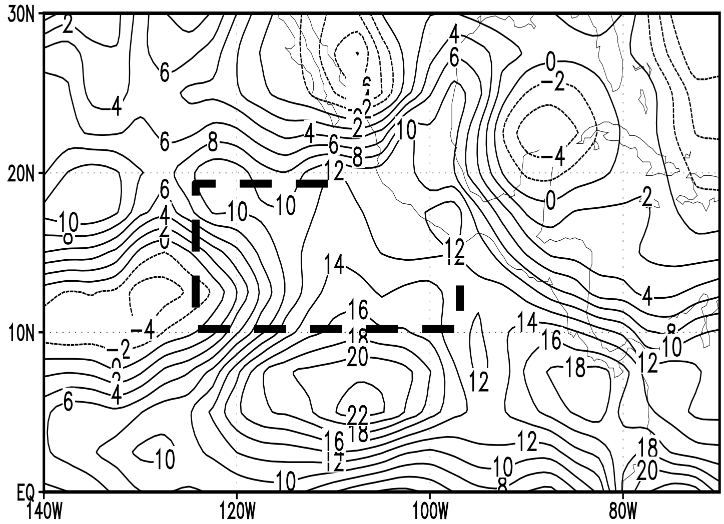

Fig. 14. 1992 minus 1977 seasonal mean 500mb relative humidity (%). Solid (dashed) contours denote positive (negative) values. Dashed lines circle the cyclogenesis region.

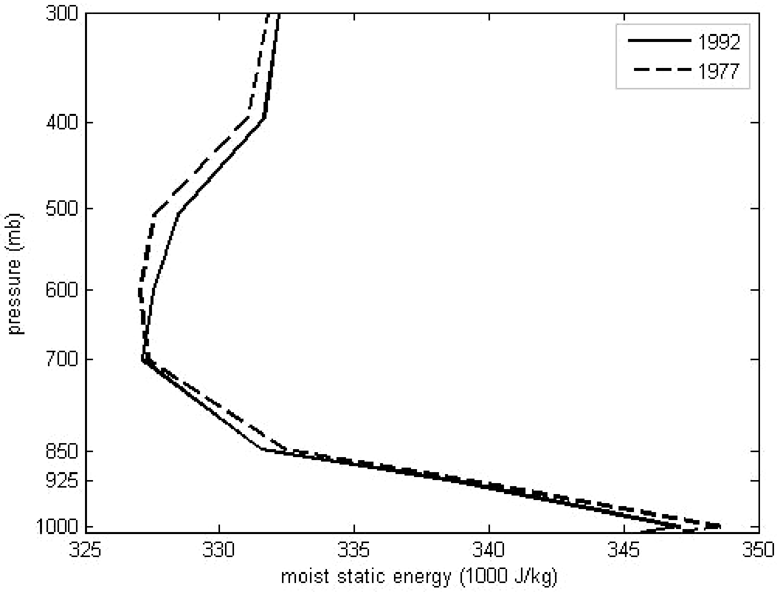

Fig. 15. Vertical profile of seasonal mean moist static energy averaged over 90-110^{o}W and 10-20^{o}N in 1992 (solid) and 1977(dashed).

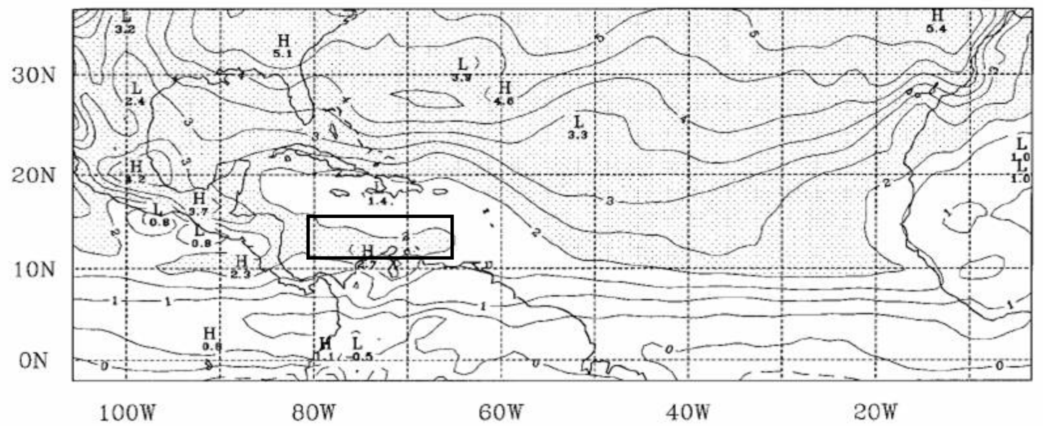

Fig. 16. 1991 Seasonal mean (15 Jun.-30 Sept.) PV ($10^{-7}m^2Ks^{-1}kg^{-1}$) on 310K isentropic surface (Molinari 1997). Areas with values greater than 2 are shaded.

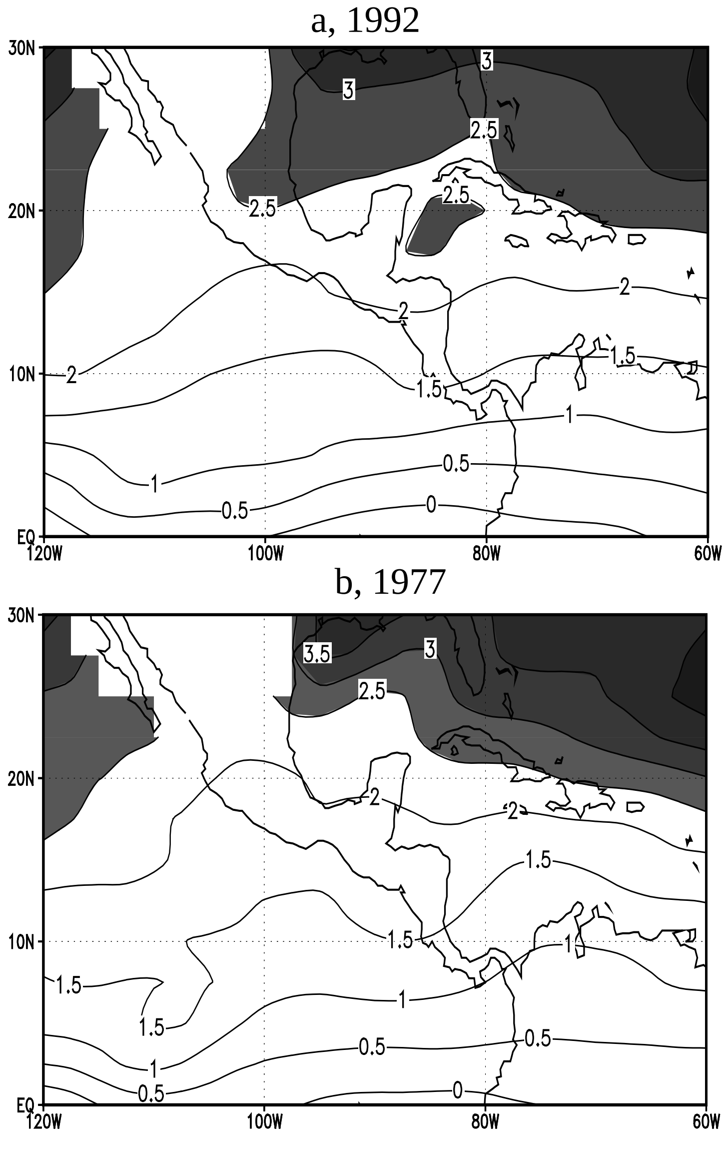

Fig. 17. Seasonal mean PV ($10^{-7}m^2Ks^{-1}kg^{-1}$) on 310K isentropic surface in (a) 1992 and (b) 1977. Areas with values greater than 2.5 are shaded.

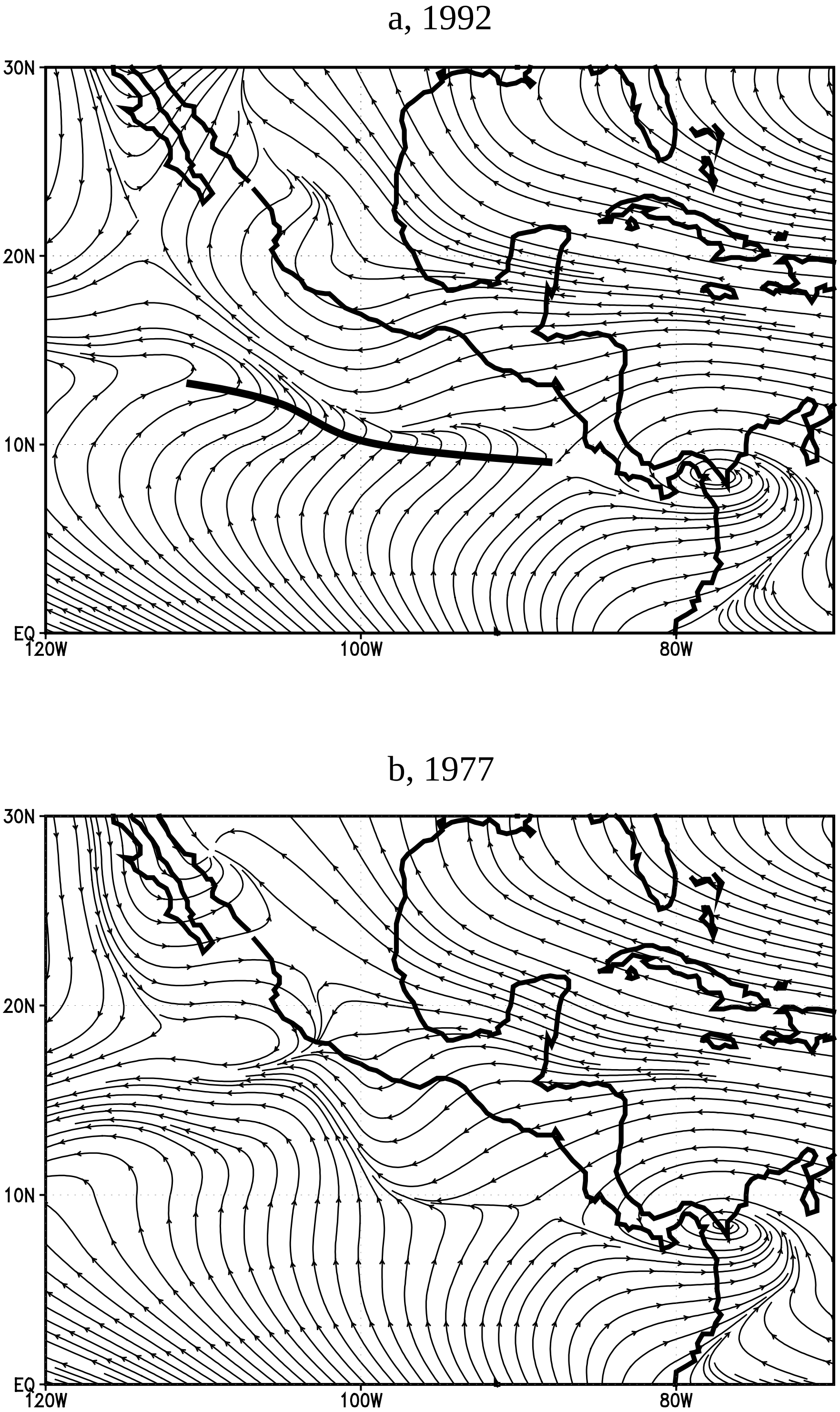

Fig. 18. Seasonal mean 925mb stream line in (a) 1992 and (b) 1977. Monsoon trough is denoted by the bold solid curve in (a).

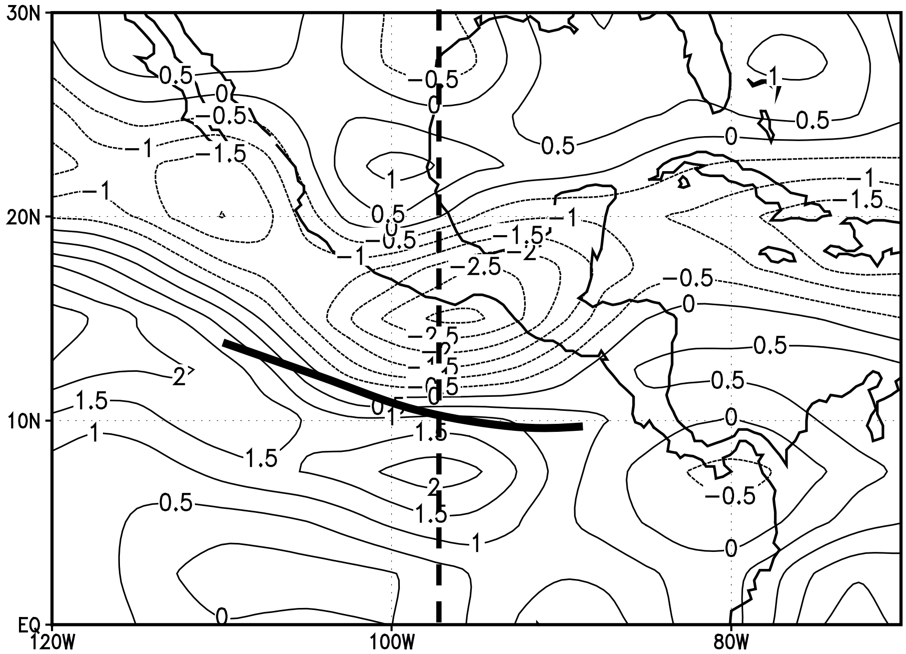

Fig. 19. 1992 minus 1977 seasonal mean 925mb zonal wind (m s^{-1}). Dashed line indicates 97^{o}W. Solid curve denotes the position of the monsoon trough in 1992. Solid (dashed) contours denote positive (negative) values.

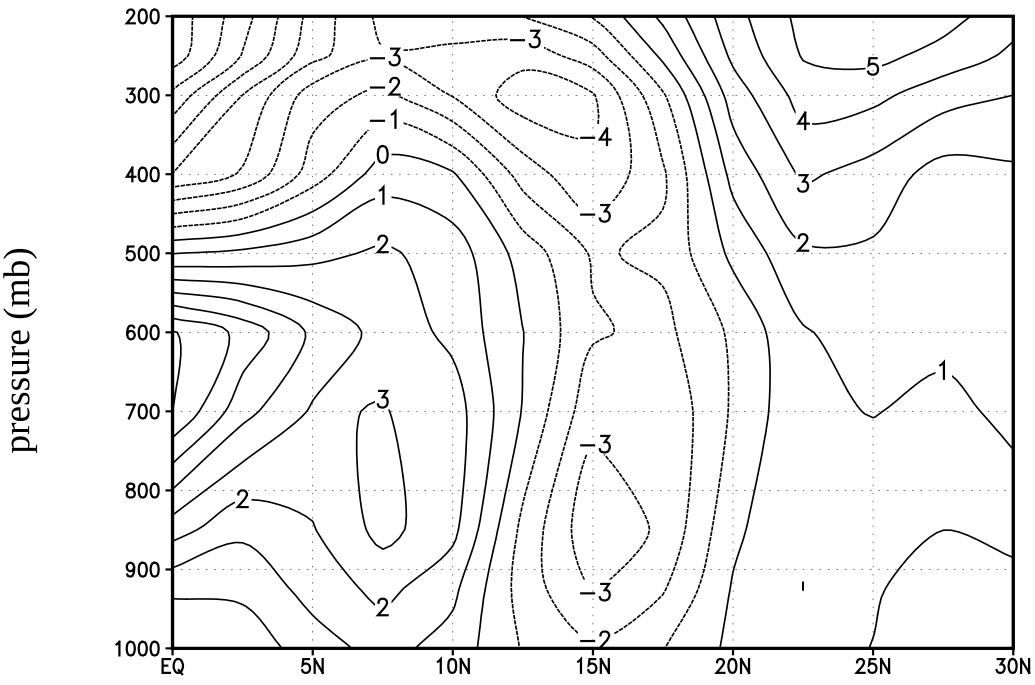

Fig. 20. Latitude-height cross section of 1992 minus 1977 seasonal mean zonal wind (m s^{-1}) along 97^{o}W. Solid (dashed) contours denote positive (negative) values.

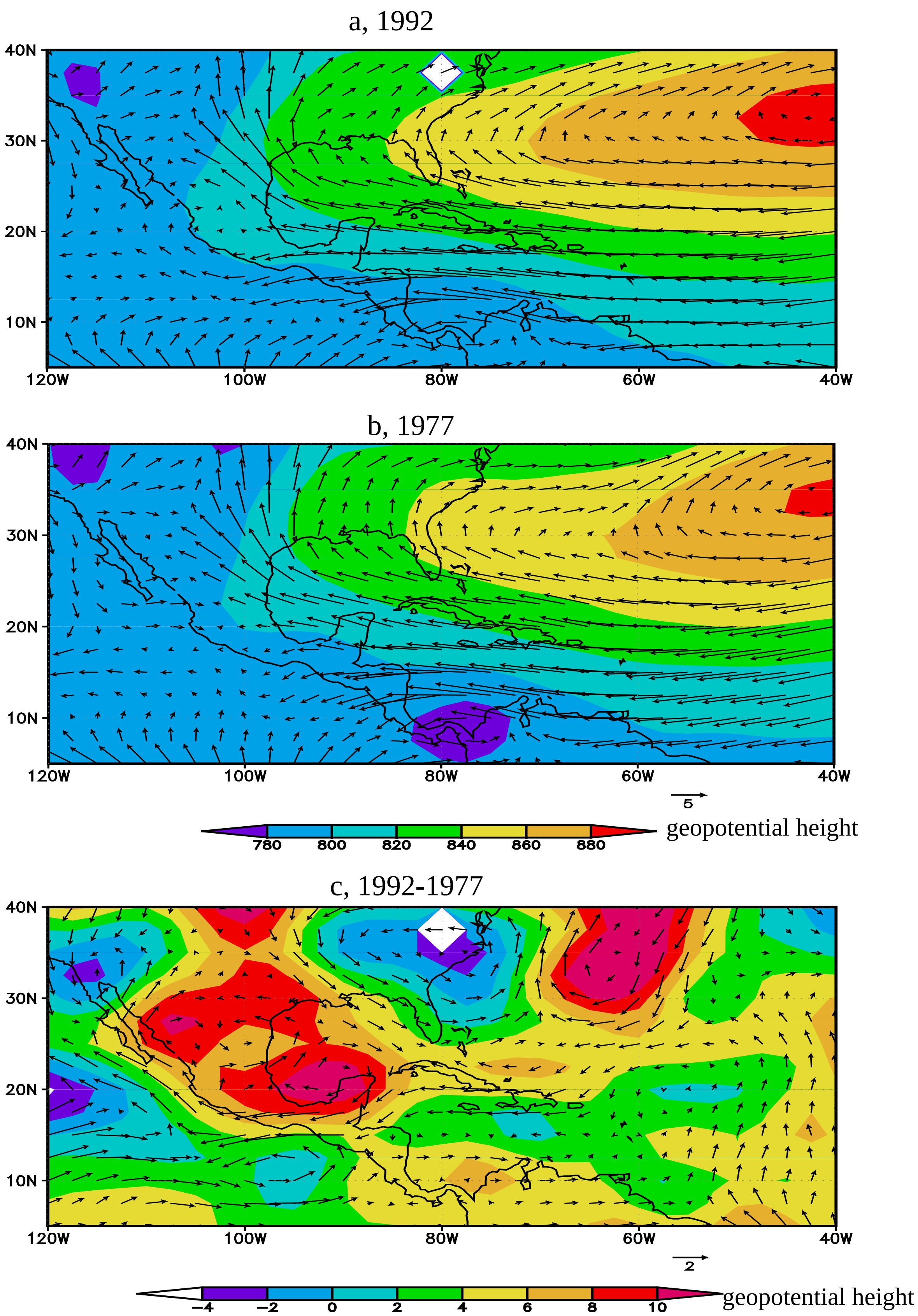

Fig. 21. Seasonal mean 925mb geopotential height (m) and winds (m s^{-1}) in (a) 1992, (b) 1977, and (c) 1992 minus 1977.

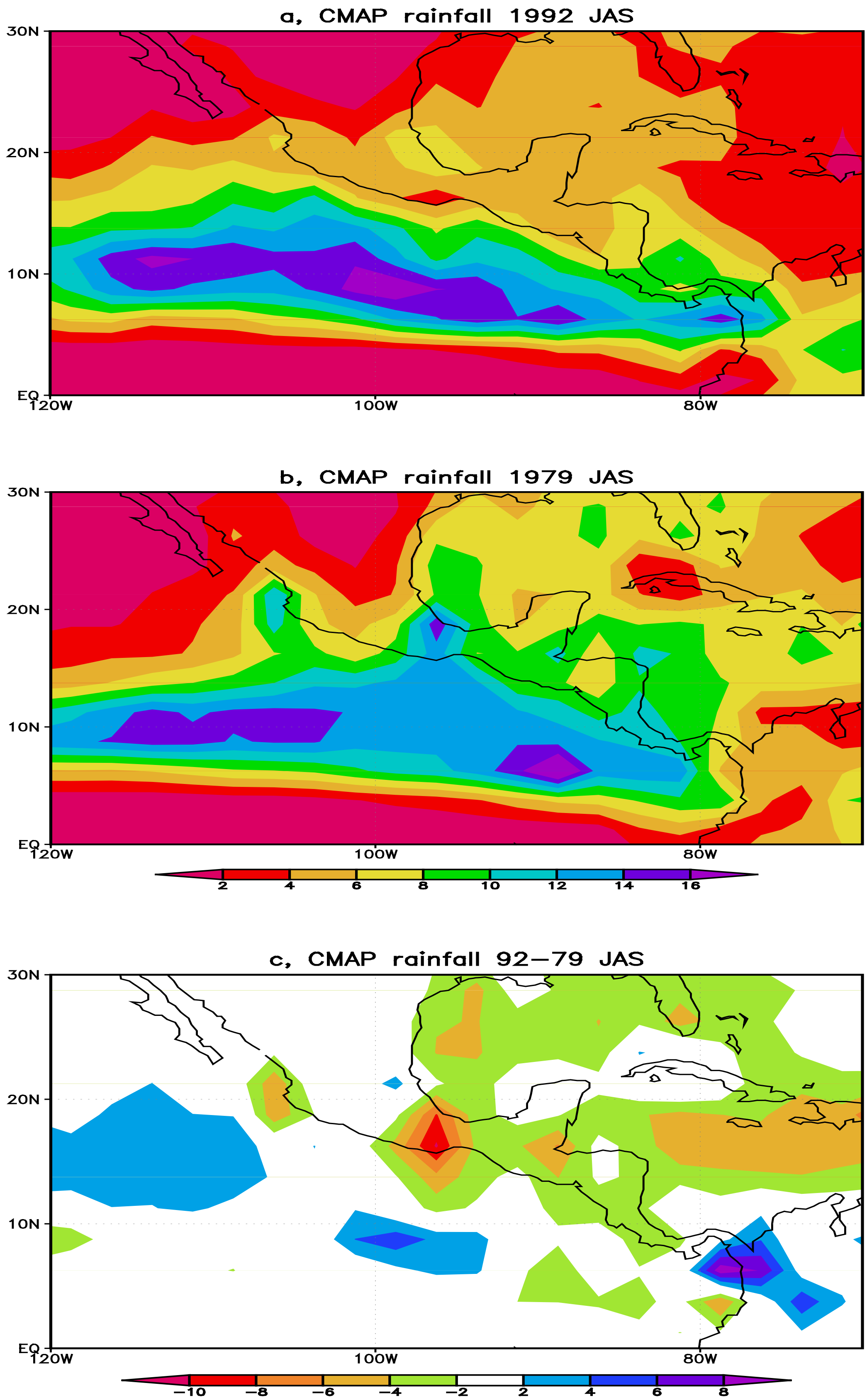

Fig. 22. Seasonal mean CMAP precipitation (mm day^{-1}) of (a) 1992, (b) 1979, and (c) 1992 minus 1979.

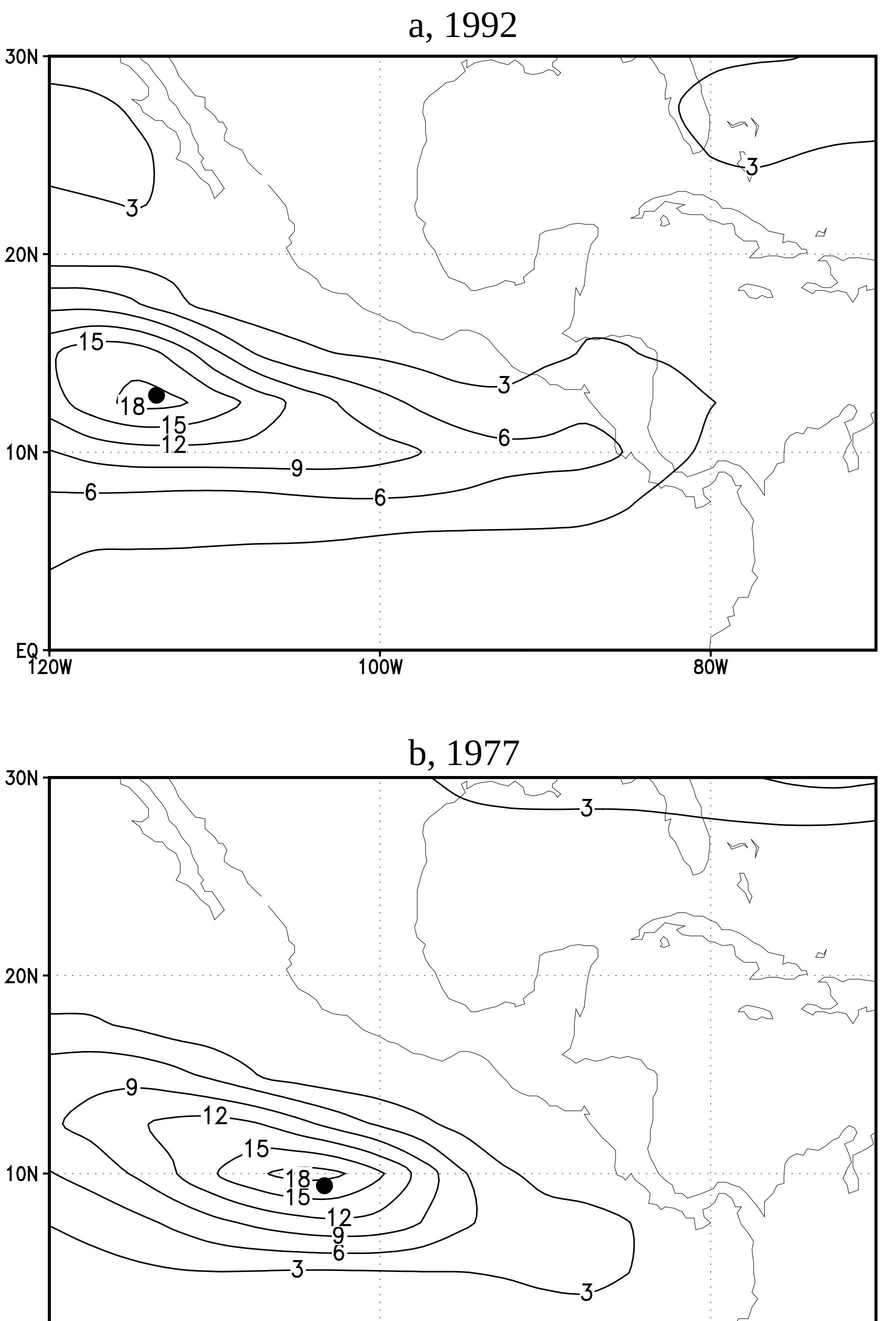

Fig. 23. Variance of 30-50-day filtered 850mb zonal wind anomalies ($m^2\ s^{-2}$) during JAS in (a) 1992 and (b) 1977. Solid dots denote locations of maximum values in each year.

a, 1992 JJASO

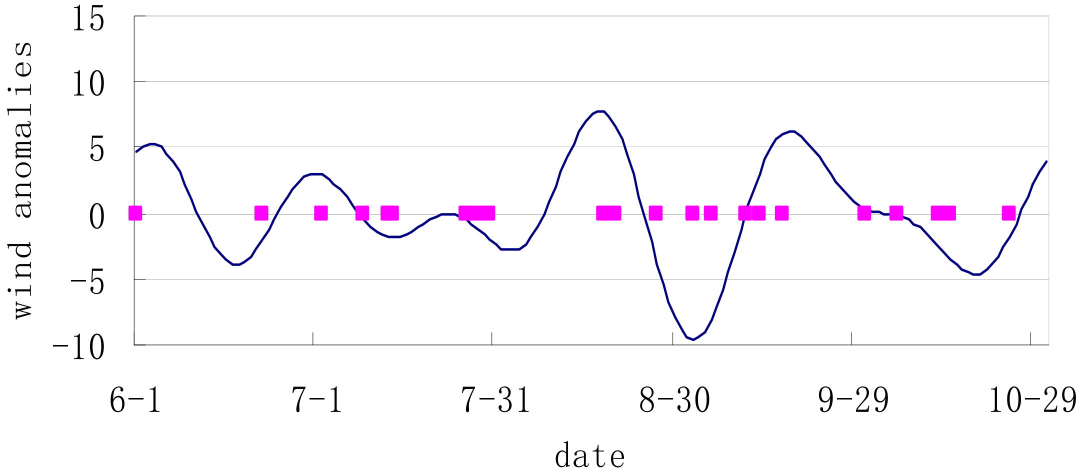

b, 1977 JJASO

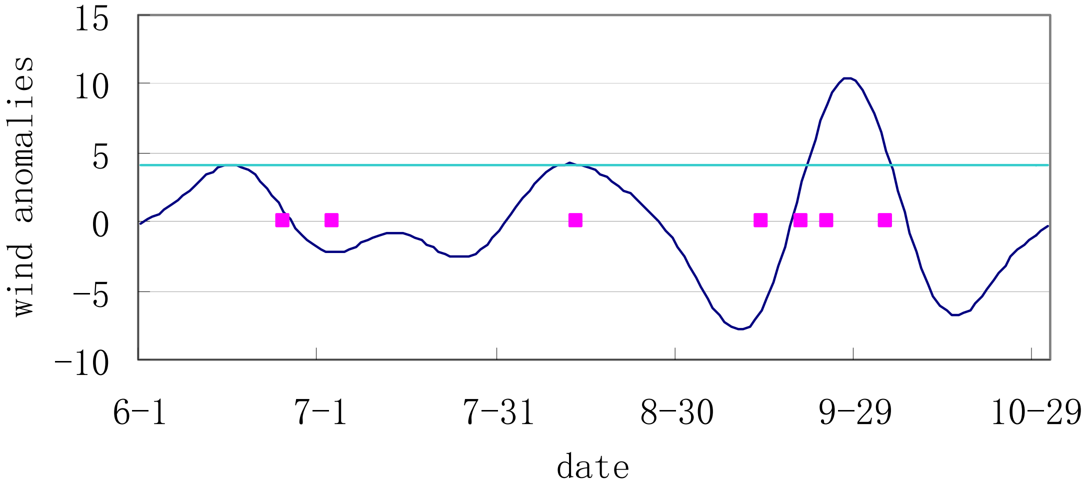

Fig. 24. 30-50-day filtered time series of 850mb zonal wind anomalies (m s^{-1}) in JJASO of (a) 1992 and (b) 1977 over the locations denoted by the solid dots in Fig. 23. Solid squares denote the timing of cyclogenesis.

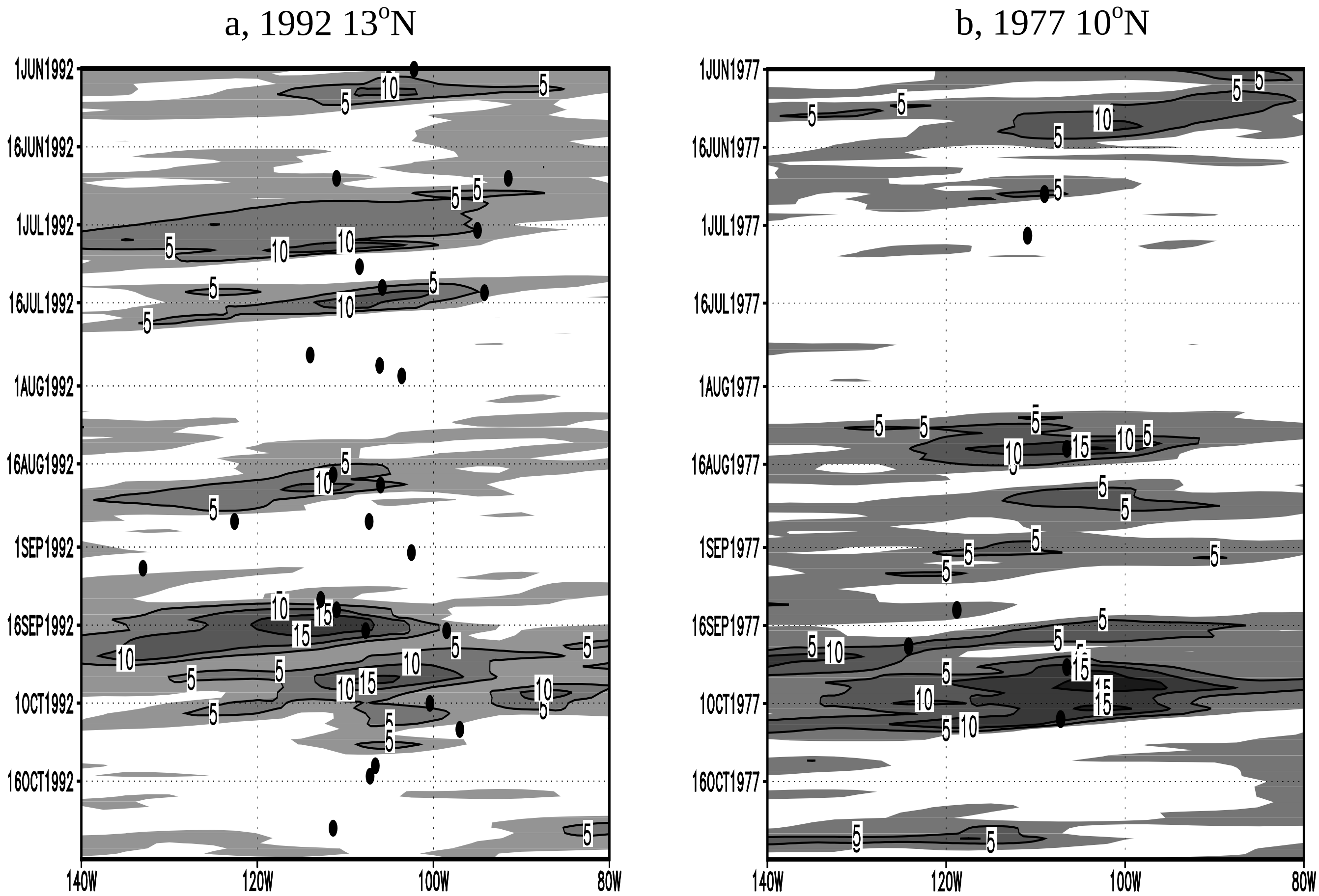

Fig. 25. Time-longitude cross section of 850mb zonal wind anomalies during JJASO in (a) 1992 along 13°N and (b) 1977 along 10°N. Only positive values are shown and shaded. Contours are every 5 m s^{-1}. Solid dots denote the timing and longitudes of cyclogenesis.

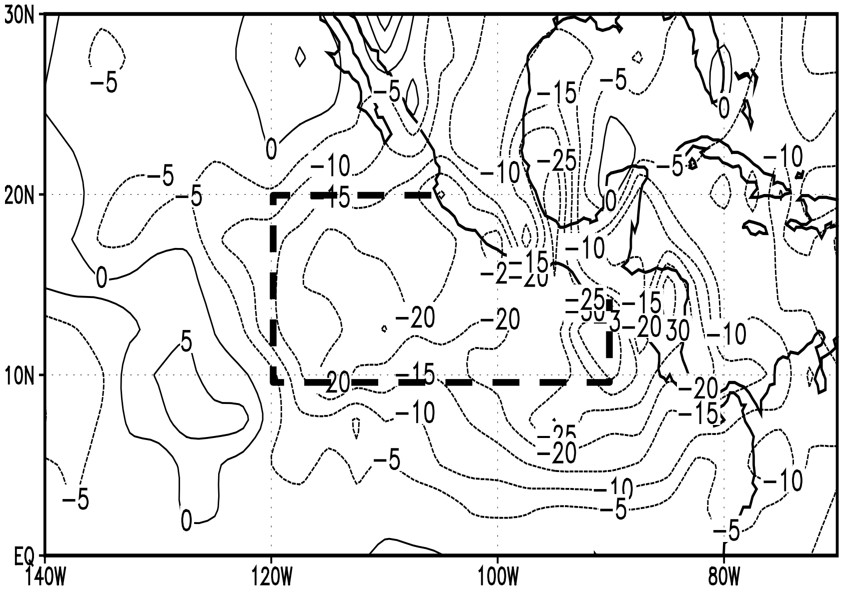

Fig. 26. 1992 minus 1977 seasonal mean OLR (W m^{-2}). Solid (dashed) contours denote positive (negative) values. Dashed lines circle cyclogenesis region.

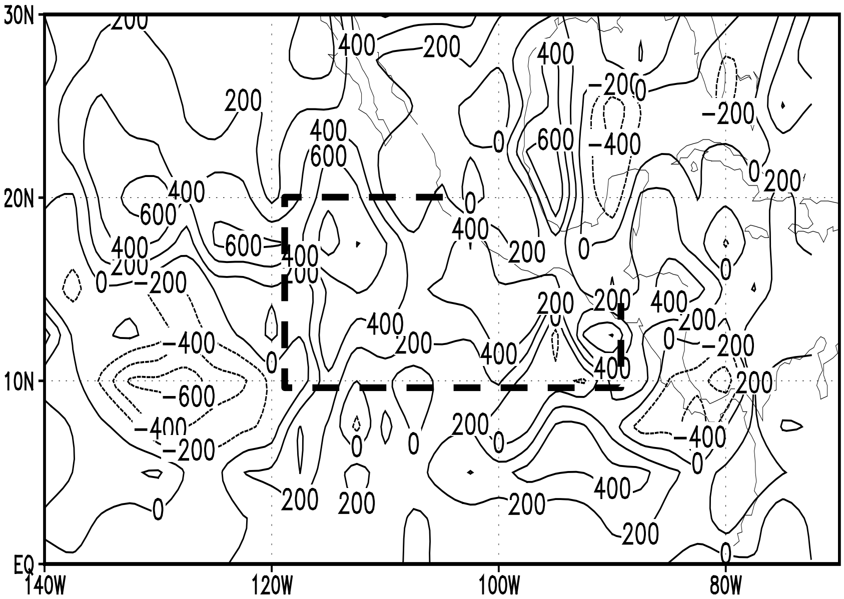

Fig. 27. 1992 minus 1977 OLR variance (W^2 m^{-4}) during JAS. Solid (dashed) contours denote positive (negative) values. Dashed lines circle cyclogenesis region.

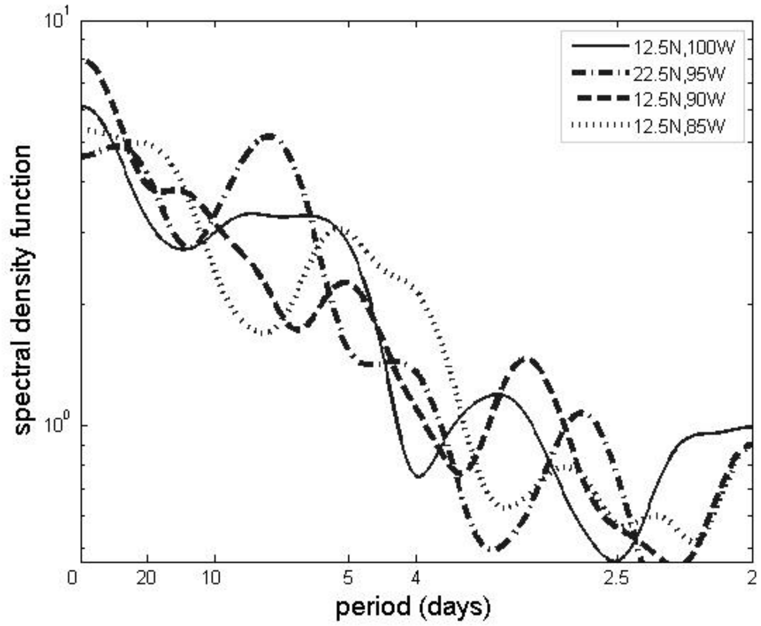

Fig. 28. Spectral density functions of OLR during June-October in 1992, over 12.5°N and 100°W, 22.5°N and 95°W, 12.5°N and 90°W, and 12.5°N and 85°W.

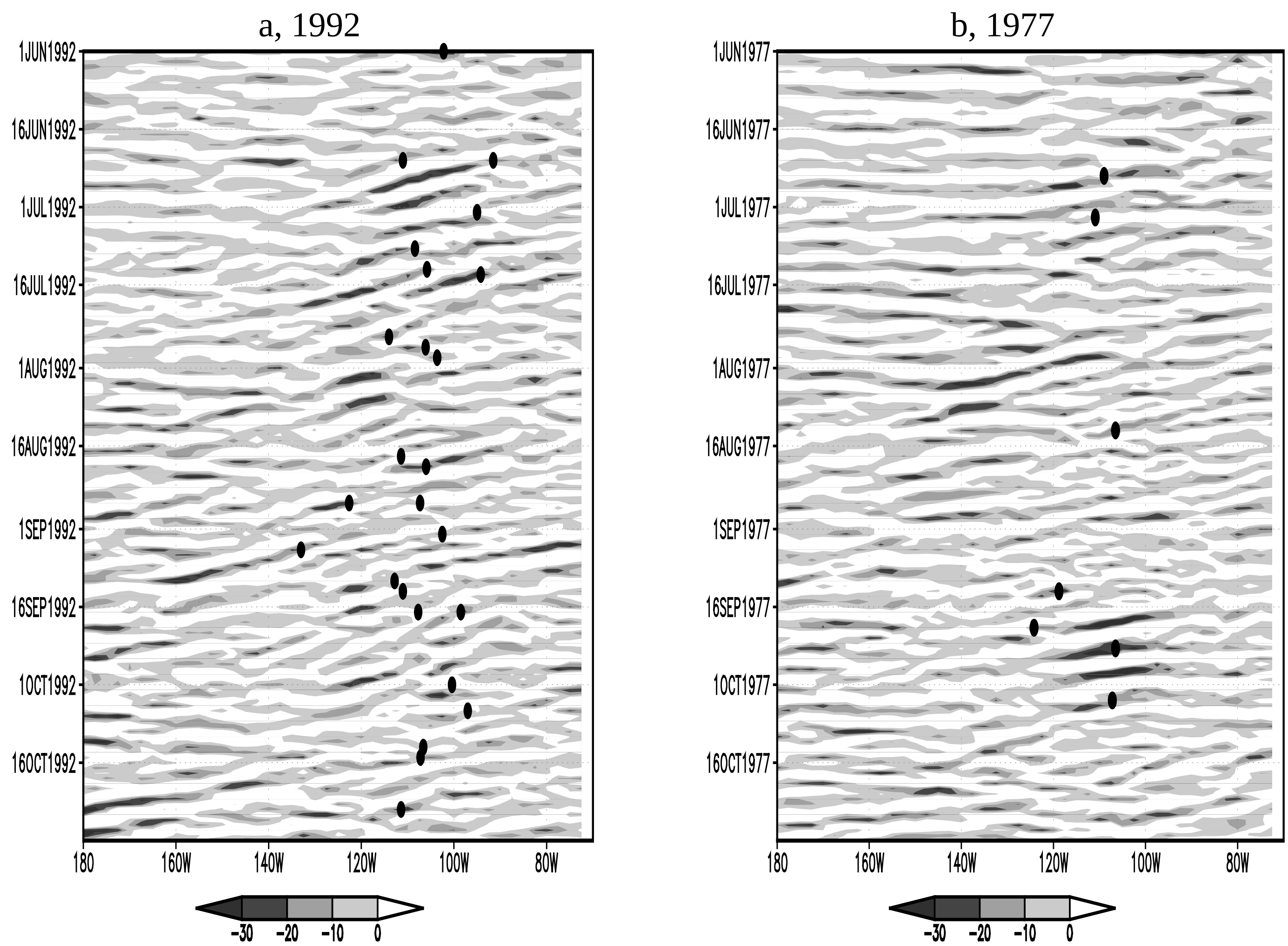

Fig. 29. Time-longitude cross section of (a) 1992 and (b) 1977 4-10-day filtered OLR anomalies (W m^{-2}) averaged between 10-20°N. Only areas with negative values are shaded. Solid dots denote timing and longitudes of cyclogenesis.